Dye-sensitized photosupercapacitor with carbon-based materials as the intermediate electrode

DYE-SENSITIZED PHOTOSUPERCAPACITOR WITH CARBON-BASED MATERIALS AS THE INTERMEDIATE ELECTRODE

A Thesis by

Victoria I. Bishop

Bachelor of Science, Wichita State University, 2022

Submitted to the Department of Mechanical Engineering
and the faculty of the Graduate School of
Wichita State University
in partial fulfillment of
the requirements for the degree of
Master of Science

December 2023

DYE-SENSITIZED PHOTOSUPERCAPACITOR WITH CARBON-BASED MATERIALS AS THE INTERMEDIATE ELECTRODE

The following faculty members have examined the final copy of this thesis for form and content and recommended that it be accepted in partial fulfilment of the requirement for the degree of Master of Science, with a major in Mechanical Engineering.

_____

Wei Wei, Committee Chair

_____

Bin Li, Committee Member

_____

Wujun Si, Committee Member

DEDICATION

To everyone who believed in me

Necessity is the mother of invention

ACKNOWLEDGMENTS

I would like to express my deepest gratitude to my advisor, Dr. Wei Wei, for her guidance, support, and encouragement. I would also like to thank the members of my committee, Dr. Bin Li and Dr. Wujun Si for their helpful comments and advice on this project. I am also grateful to my lab mates, for their assistance in lab work, and patience for my many questions regarding writing and editing. Additionally I would like to extend my gratitude to the National Aeronautics and Space Administration for funding this research. Finally, I could not have undertaken this endeavor without the support of my family, including my parents and younger sister.

ABSTRACT

Due to the growing environmental crisis, developing new methods of generating and storing renewable energy is more important than ever. Solar is among the most promising renewable methods; however, it has some critical weaknesses. To addresses these weaknesses, methods of storing energy in the form of batteries and supercapacitors have been evaluated. The overall goal for such devices is to integrate the solar cell and storage device into a single electronic device that can account for power fluctuations, and provide energy when requirements are the highest.

Third generation solar cells are ideal for the potential applications these devices would have. This generation includes dye-sensitized solar cells (DSSCs), perovskite solar cells, organic solar cells, and quantum-dot solar cells. Supercapacitors are a developing technology that are also ideal for the potential applications. Combining third generation solar cells like DSSCs with supercapacitors would result in an inexpensive device capable of converting and storing solar energy in a simple way.

In this thesis, four commercial carbon materials were investigated as electrodes for monolithic DSSC-supercapacitor devices and directly compared for the first time. The objective of this research is to determine if inexpensive carbon-based materials are effective and competitive as electrodes in these devices. The four materials chosen are activated carbon, mesoporous carbon, graphite, and graphene. Of these four materials, graphite had the poorest power conversion efficiency after integration at 1.43%, and graphene had the lowest mass specific capacitance of 13.0 F g^{-1}, attributed to the simplistic fabrication methods. In comparison, Mesoporous Carbon achieved the best integrated performance with an integrated power conversion efficiency of 3.10%, a photocurrent of 1.37 mA, and a post-integration mass specific capacitance of 40.0 F g^{-1}.

TABLE OF CONTENTS

LIST OF TABLES

LIST OF FIGURES

LIST OF FIGURES (continued)

Figure Page

LIST OF SYMBOLS AND ABBREVIATIONS

AC	Activated Carbon
CE	Counter Electrode
CNT	Carbon Nanotube
C_{sp}	Specific Capacitance
CV	Cyclic Voltammetry
D35	(E)-3-(5-(4-(bis(2',4'-dibutoxy-[1,1'-biphenyl]-4-yl)amino)phenyl)thiophen-2-yl)-2-cyanoacrylic acid
DSSC	Dye-Sensitized Solar Cell
DSSCSC	Dye-Sensitized Solar Cell and Supercapacitor
EDLC	Electric Double-Layer Capacitor
E_g	Energy Density
EMIBF4	1-Ethyl-3-methylimidazolium tetrafluoroborate
FTO	Fluorine-doped Tin Oxide
GCD	Galvanostatic Charge/Discharge
GO	Graphene Oxide
HOMO	Highest Occupied Molecular Orbital
IE	Intermediate Electrode
IT	Constant-Current Test
IV	Current-Voltage Test
J_{sc}	Short Circuit Current
KOH	Potassium Hydroxide
LIB	Lithium-Ion Battery

LUMO	Lowest Unoccupied Molecular Orbital
MACNT	Micro-array Carbon Nanotubes
MC	Mesoporous Carbon
MWCNT	Multi-walled Carbon Nanotubes
N3	cis-Bis(isothiocyanto)bis(2,2'-bipyridyl-4,4'-dicarboxylato ruthenium(II))
P3HT	poly(3-hexythiophene-2,5-diyl)
PAAQ	Poly(1-aminoanthraquinone)
PANI	Polyaniline
PC	Polycarbonate
PCE	Power Conversion Efficiency, also η_{sc}
PEDOT	Poly(3,4-ethylenedioxythiophene)
PEO	Polyethylene Glycol
P_g	Power Density
PProDOT	Poly(3,4-(2,2-dimethylpropylenedioxy)thiophene)
Ppy	Polypyrrole
PSS	Polystyrene sulfonate
PTFE	Polytetrafluoroethylene
PVA	Poly(vinyl alcohol)
PVDF	Polyvinyl difluoride
PVP	polyvinylpyrrolidone
Pyr14TFSI	1-Butyl-1-methylpyrrolidinium bis(trifluoromethyl sulfonyl)imide
SC	Solar Cell
SEM	Scanning Electron Microscope

TBAI	Tetrabutylammonium iodide
TEABF4	Tetraethylammonium tetrafluoroborate
V_{oc}	Open Circuit Voltage
VT	Constant-Voltage Test
XRD	X-ray Diffraction
ZNWA	Zinc Nanowire Array

CHAPTER 1

INTRODUCTION

The entire globe is facing extreme environmental challenges such as climate change, natural resource depletion, overpopulation and more. The increasing energy demand due to the growing population and the growing amount of devices that require electricity has resulted in a need for state-of-the art innovations in electricity generation that are not reliant on fossil fuels. Fossil fuels and any energy generation approach that uses them, exacerbates the issues of global warming and resource depletion [1, 2]. To address these issues of depleting resources and promote a positive change in greenhouse emissions, novel new methods of energy generation that are renewable and safe need to be created [3]. Among the many types of renewable sources of energy, ranging from wind and wave to biomass focused sources, solar cells (SCs) are capable of providing an enormous amount of energy that is drawn from the sun, making it abundant, clean, and cheap [4, 5].

Despite their positive attributes, SCs have a glaring weakness: such devices cannot create energy when it is cloudy or at night, times when energy usage is typically higher, and they are inefficient at converting energy to a usage form compared to the amount of solar energy that strikes the earth's surface [6]. Storing the excess energy generated during the day to be used when there is a higher demand is a critical new facet of renewable energy that also needs to be addressed. Several options for this storage exist, including chemical, mechanical, electromagnetic, or thermal methods [7]. Chemical or electrochemical devices such as batteries and supercapacitors have proven to be the most compatible with SCs, serving to store the energy converted and unutilized during the day until such times that it is needed [7-10]. Lithium-ion batteries (LIBs) are a rapidly

growing technology that have served well as reusable energy storage, appearing in everyday electronics, and electric vehicles. However, LIBs have a limited number of charge/discharge cycles and thus require replacement. Critically, LIBs require recycling once they reach the end of their life-cycle, which is made difficult and expensive by the evolving materials used in their manufacture, leading to many LIBs being manufactured from non-recycled materials [11]. Supercapacitors in comparison have lower energy density than LIBs, but are being used increasingly often as energy storage devices due to their long life-cycle, high stability, and high power density [12-14].

The integration of SCs and supercapacitors is a promising and innovative field that is expected to yield novel new devices capable of converting and storing energy within one device [15, 16]. Understanding the fundamentals of these devices and their functionality is beneficial to understanding potential processes of integration. SCs, also called photovoltaics, traditionally convert the sun's energy into electricity by the photoelectric effect. The photoelectric effect, discovered by Heinrich Rudolf Hertz in 1887 – also attributed to many other scientists active during this century – arises when photons from sunlight are absorbed by a semiconductor material, generating a charge, exhibited in Figure 1 [17]. When photons hit the semiconductor, the atoms within the material transfer the energy from the photons to the unexcited electrons, exciting them. Once a number of electrons are excited, the unbalanced charge at either electrode forces the electrons to be move in a uniform direction, becoming an electric current [18].

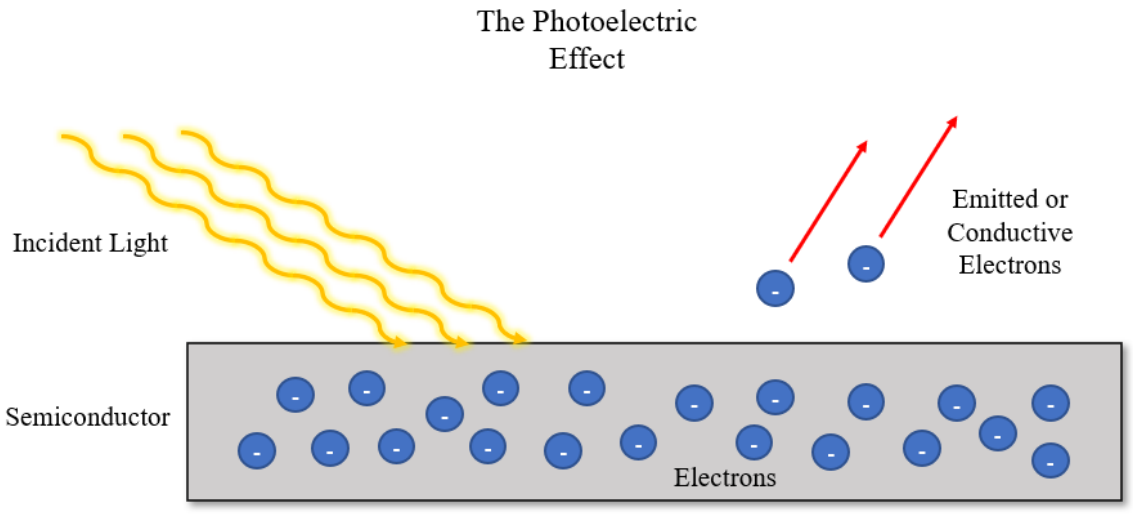

Figure 1: The photoelectric effect explained by Heinrich Rudolf Hertz in 1887.

Three generations of photovoltaics have been manufactured on the research and commercial scales, outlined in Figure 2. First generation photovoltaics use the photoelectric effect to generate a current through specifically doped-silicon semiconductors: p-type semiconductors contain an excess of holes that can move freely, and the n-type semiconductors which contain an excess number of electrons that can move freely [19]. Second generation photovoltaics utilize thin film photoelectrodes fabricated from silicon, cadmium, telluride, and copper indium gallium di-selenide. These second-generation cells can achieve high stability and efficiency compared to the original first generation cells, but utilize expensive and potentially toxic materials compared to the newer generations of photovoltaics [20]. Third-generation photovoltaics are based on inexpensive semiconductive materials, utilizing new and novel materials to take advantage of the photoelectric effect and lower production costs of SCs [21, 22]. Among third-generation SCs, Dye-Sensitized Solar Cells (DSSCs) are among the most versatile being low-cost alternatives to existing silicon-based cells, with additional low-light conversion capabilities [23-26]. Consisting of a semiconductive photoanode, a photo-active dye, a redox electrolyte, and a counter electrode (CE),

these cells have achieved reliable photo-conversion efficiencies (PCE) of upwards of 10% in the last decade of research [24, 25]. These cells have often utilized TiO_2 as the semiconductive material, a Ruthenium-based dye, iodide/triiodide (I^-/I^{3-}) redox electrolyte, and platinum CE to great effect, with many alternative materials for each component being studied. Most relative to this study, alternative CE materials have included carbon-based materials, favored for their low cost, high stability, and large surface area [27, 28].

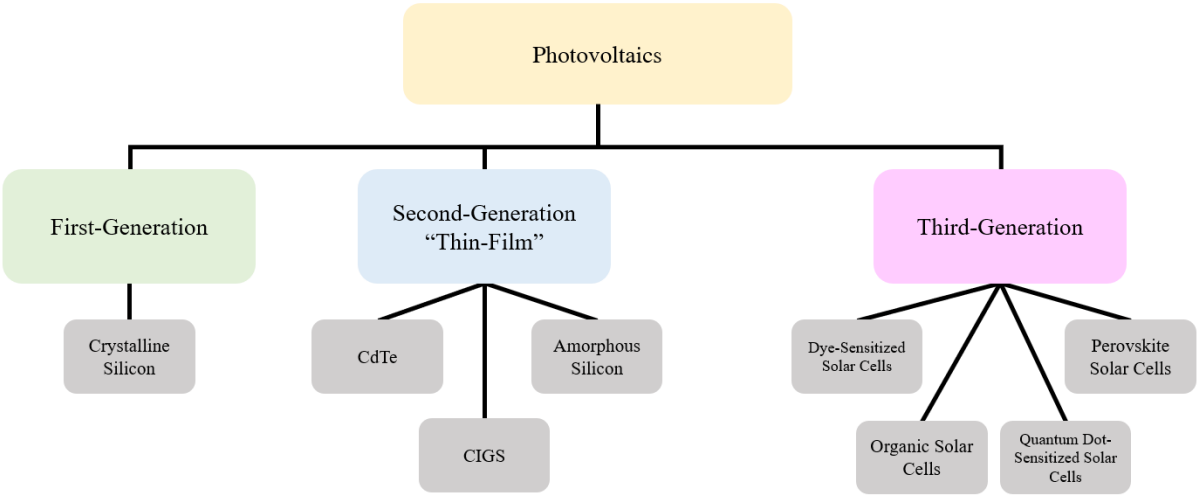

Figure 2: The three generations of solar cells, with the current representative cells of each generation.

Supercapacitors combine the better features of batteries and capacitors to hold large amounts of power that can charged and discharge quickly and efficiently. Specifically, energy is stored within a supercapacitor in one of three ways – through an electric double layer, pseudo-capacitance, or hybrid mechanisms – between two symmetric or asymmetric plates that are separated by a porous electrolyte or membrane [29-31]. Pseudocapacitors use symmetric electrodes to store energy through Faradaic reactions, where the charge is transferred through the redox reaction [30, 32]. Electrode materials for Pseudocapacitors have included metal oxides and

conducting polymers, resulting in high capacitance and energy density but lower life cycles and stability [33]. Electric double layer capacitors (EDLCs) store energy as a layer of accumulated ions at the electrode/electrolyte interface, using non-redox electrolytes and symmetric electrodes – notably activated carbon (AC) – to achieve longer life cycles, fast charge/discharge, and high power-density [30, 33]. Hybrid supercapacitors combine the mechanisms for EDLCs and Pseudocapacitors into one device. This type of device is often fabricated with redox-capable electrolytes and asymmetric electrodes composed of pseudocapacitive and carbon-based materials, achieving greater energy storage properties and improved stability compared to pseudocapacitors, making this device functionally similar to a battery [14].

Integrated devices can combine solar cells like DSSCs and supercapacitors into one device. Much research has been performed on combined DSSCs and supercapacitors, beginning in 2004 with a two-electrode photocapacitor using a TiO_2 photoanode and an AC CE and EDLC, achieving a charging voltage of 0.45 V and an areal specific capacitance of 0.65 F cm^{-2} [34]. A three-electrode device based on the same materials followed after, addressing the issues in the previous iteration, improving the conversion and storage to an 0.8 V charging voltage and a 47 µWh cm^{-2} energy density, five times greater than the two-electrode device [35]. Subsequent studies have generally focused on the three-electrode format, where an intermediate electrode separates the DSSC and supercapacitor modules, allowing for each section to use separate electrolytes. Devices with this format have shown increased performance over the two-electrode devices, and been fabricated using traditional methods, as well as into flexible and textile devices [27, 28, 36].

1.1: Applications

Solar Cells and Integrated devices are highly desired not only for their ability to generate clean and abundant energy, but for their multiple applications. Solar cells can be applied anywhere there is abundant sun to generate clean energy, with the simplest application being utility power generation. Since solar cells can be applied anywhere, not necessitating a connection to the existing energy grid to provide electricity, smaller devices can be good for emergency situations. Solar cells are also good for remote locations where there is not already a grid connection, or where a grid connection would be difficult to achieve. One such application for these devices is in space, where photons from the sun are abundant at nearly all times while in orbit around the earth [37].

Due to the potentially transparent nature of DSSCs, they have been fabricated as integral parts of buildings and greenhouses to produce energy unobtrusively [38, 39]. These can include windows and skylights, shingles, canopies, and facades. Integrated and non-integrated devices can be specially manufactured into smart windows, that through the use of specific photoelectrode materials, undergo a color change when a photo-current is generated, reducing energy costs related to the building [40, 41]. DSSCs can also be used internally to power small devices due to the wide nature of light that the cell is sensitive to, performing better in low light conditions inside than other types of cells and connected to bags and furniture to charge mobile devices [39].

Small devices and sensors are the largest draw for integrated SC and supercapacitor devices [42]. They are expected to be of use for wearable electronics that can include mobile devices and medical sensors, where it is impractical to have a fluctuating energy source from the SC alone, large batteries, or require frequent conventional charging [43]. It is due to these varied applications that integrated systems of energy storage are highly desired.

1.2: Research Objectives

The objective for this research is to determine the utility and performance of commercial materials as electrodes for an integrated, monolithic DSSC and supercapacitor device. The commercial materials are known to be capable low-cost alternatives to traditional DSSC and supercapacitor electrodes. For each commercial material selected, the performance will be analyzed considering several conditions. The solar cell module will be analyzed by the open circuit voltage, short circuit current, fill factor, and power conversion efficiency. The supercapacitor module fabricated with the commercial materials will be analyzed by the mass specific capacitance, the energy density, and the power density. The integrated device will be analyzed by the integrated photocurrent, charging voltage, power conversion efficiency, and the integrated mass specific capacitance. These performance metrics will be discussed in detail in Chapter 2.1 and 2.2.

The ultimate goal of this project is to determine if already existing commercial materials are compatible with the configuration chosen to fabricate this device. As such, the materials must show viability based on their performance metrics. The information gathered here should also provide important knowledge on how these types of devices can be tested, what performance metrics should be analyzed, and how these devices function in order to optimize them for eventual commercialization.

1.3: Thesis Outline

This thesis is divided into the following chapters:

Chapter 2 is a literature review on the mechanisms of DSSCs and supercapacitors, and the integrated devices made from these structures. Chapter 3 is the experimental section outlining the

materials used, how the devices in this thesis were manufactured, and how the devices were tested. Chapter 4 discusses the results of the tested devices based on their performance metrics. Chapter 5 summarizes the results of the study and chapter 6 will discuss possible future work in this field of study.

CHAPTER 2

LITERATURE REVIEW

2.1: Dye Sensitized Solar Cell Working Mechanism

Dye-Sensitized solar cells have an extensive history of research, resulting in a well understood structure and mechanism. The main components of the DSSC are the conductive glass or polymer substrates, a photoanode containing a semi-conductive material sensitized by an appropriate dye, a redox-reaction capable electrolyte, and a counter electrode (CE) with catalytic properties. The structure of such cells are described in Figure 3. The dye-sensitized photoanode that gives the SC its name typically consists of a semi-conductive metal oxide and a light activated dye that has bonded to the surface of the semiconductor particles. Various metal oxides have been utilized as the semi-conductive material, although the most common is TiO_2 due to its being inexpensive, non-toxic, and within the range of appropriate electrical properties such as the band gap [44]. Alternative materials for the photoanode have included Au-, Zn-, W-, Sn-, Ag-, and Carbon-based semiconductor particles, although this is far from an exhaustive list [45]. Additionally, the nanostructure of the photoanode material can be modified by doping the semiconductor with cationic or anionic groups or absorbance modifying nanostructures to further improve the performance [46].

The light activated dye that makes up the other half of the photoanode can consist of organic – natural or synthetic – or organometallic complexes. The requirements for the dye are that it must be capable of promoting electrons to an excited state by photons that are in or very near the visible range that makes up a large amount of the light from the sun and remain stable while it is in use. Most natural organic compounds are derived from plant matter such as fruits,

flowers, and leaves, thus being safe and inexpensive materials that contain compounds such as carotenoids, flavonoids, betalains, and chlorophyll that facilitate the photon absorption and energy conversion [44, 47, 48]. Synthetic dyes tend to be more effective than natural dyes due to their highly specialized fabrication as well as their ability to be co-sensitized, effectively absorbing a wider range of light than their natural counterparts [49, 50]. Organometallic dyes are among the most widely used and include Ruthenium complex dyes that offer the highest energy conversion performance at the cost of using expensive rare metals and decreased stability in humid environments [45, 49, 51].

The liquid redox-capable electrolyte for DSSCs can be the most unstable component within the structure, with the requirements of high stability under the varied conditions the cell could experience and capable of performing oxidation-reduction reactions with low loss over time. The most frequently used electrolyte for research on DSSCs is a liquid iodide/triiodide mixture in an organic solvent [49, 52]. Research has also begun on solid and quasi-solid electrolytes made form polymers and gel-solutions in an effort to improve the stability and conductivity of the electrolyte in varied conditions [45, 53, 54].

The final and most variable component in research on DSSCs is the CE, the performance of which has been evaluated with a wide range of materials. Some of the best performances have been achieved with platinum CEs but the metal is expensive and unsuitable for large-scale production, making the determination of an environmentally friendly and inexpensive CE material increasingly necessary. Conducting polymers, carbons, doped heteroatom, and heterojunction nanomaterials have shown great promise as a replacement for platinum and other rare metals as CEs for DSSCs, resulting in low-cost DSSCs that are easily scaled for large-scale or commercial production [52, 55].

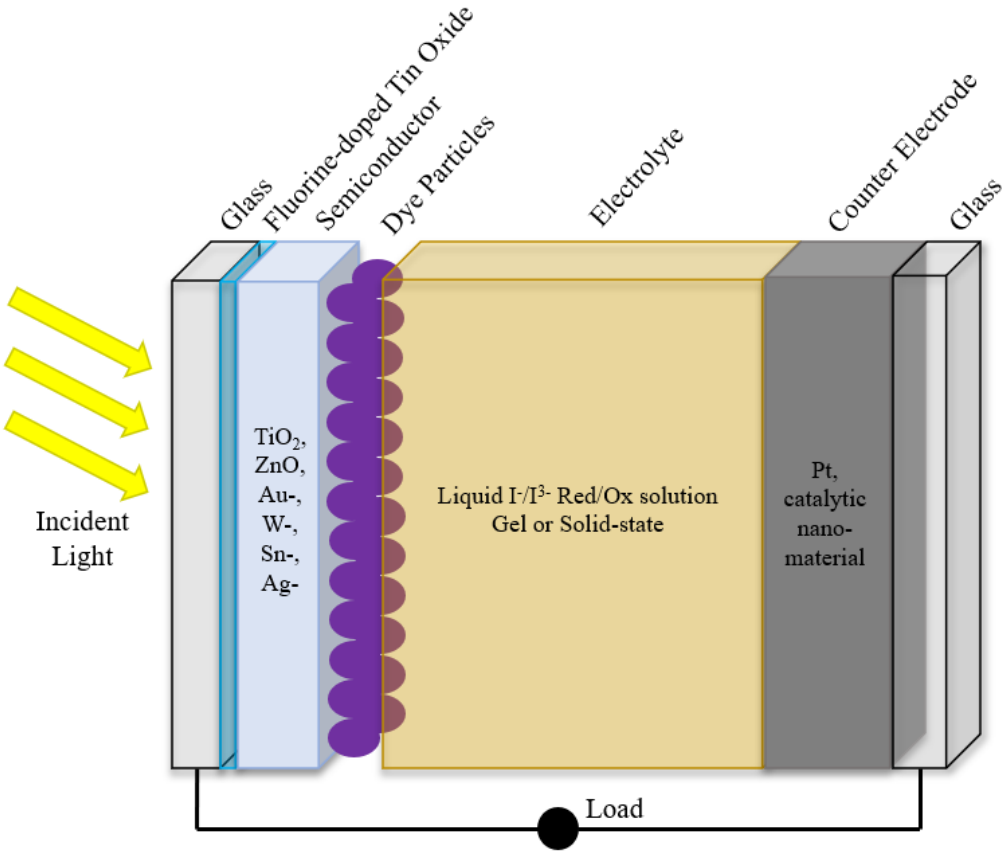

Figure 3: DSSC structure consisting of a photoelectrode made from a semiconductive metal oxide and dye particles, a redox capable electrolyte such as I^-/I^{3-}, a counter electrode, and closing glass slides coated with a layer of fluorine-doped tin oxide (FTO).

DSSCs operate based on a redox reaction that takes place between the dye, electrolyte, and CE, and mimics the process of photosynthesis. The working principles that occur are based on the processes of light absorption, charge separation, and charge collection [56]. The steps this principle follows are highlighted in the diagram in Figure 4. First, photons must strike the surface of the DSSC, passing through the transparent conductive substrate where they are absorbed by the dye. Second, an electron in the dye is promoted from the highest occupied molecular orbital to the lowest unoccupied molecular orbital, creating an electron-hole pair. Third, the excited electron

moves into the conduction band of the semi-conductive photoanode material and is then transferred to the conductive substrate and carried to the load. Fourth, the now existing hole in the dye reacts with the electrolyte in an oxidation-reduction reaction, regenerating the hole in the dye. At the same time, the electrolyte is regenerated by performing another oxidation-reduction reaction with the CE, facilitated by the electrons returning to the device from the external load [56, 57]. Theoretically, this series of reactions can continue indefinitely under optimal conditions. Realistically, the cell does not operate under optimal conditions and degrades over time. This degradation is due to internal recombinations that prevent the movement of electrons to the conduction band, and the degradation of the electrolyte – most notable for liquid state electrolytes – and dye through oxidation in air [58].

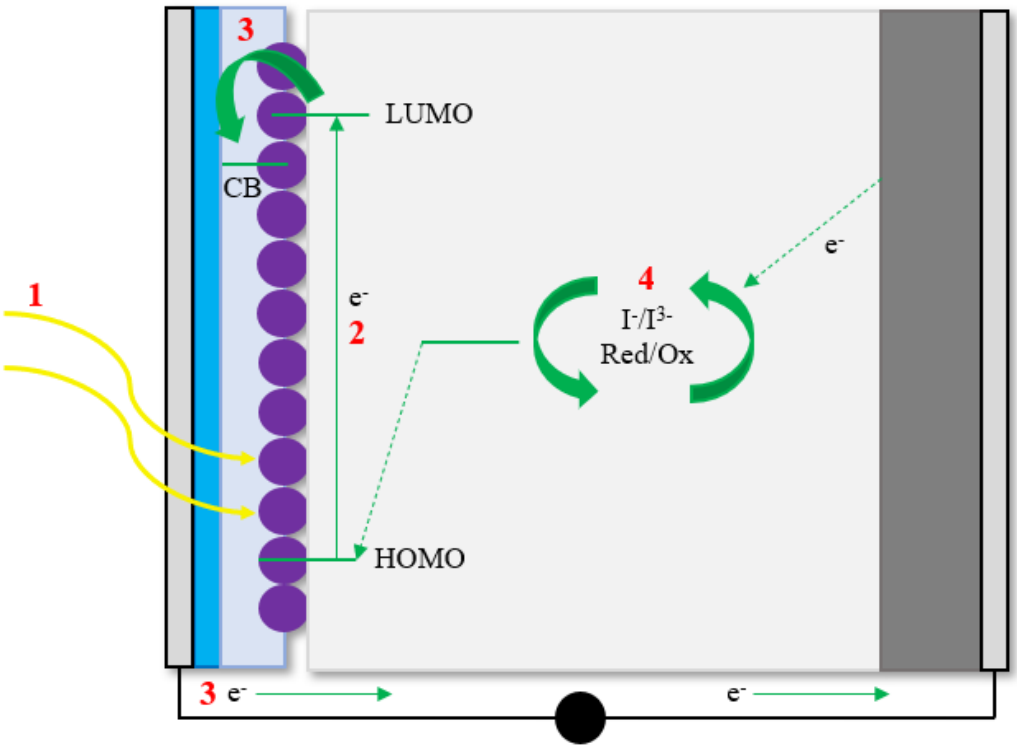

Figure 4: DSSC working mechanism. 1) Light strikes the surface and is absorbed by the dye particles. 2) An electron in the dye is excited after absorbing the energy from the photon, moving from the HOMO to the LUMO. 3) The electron is promoted to the CB of the semiconductor and transferred to the load, then back to the cell through the CE. 4) the reaction between the CE, redox electrolyte, and dye regenerates the cell.

The performance of DSSCs are evaluated based on four measured or calculated properties that are revealed by testing under simulated light at known intensities. These four properties are the open circuit voltage (V_{oc}), the short circuit current (J_{sc}), the fill factor (FF), and the power conversion efficiency (PCE). The power conversion efficiency determines how much energy input into the cell is converted to usable electrical energy and is calculated based on the other operating parameters of V_{oc}, I_{sc}, and FF. The operating parameters of V_{oc} and J_{sc} are drawn directly from the

measured current or current density-voltage data (IV), representing where the voltage across the cell when there is no current (V_{oc}) and the current across the cell when the voltage is zero (I_{sc}) [59]. The FF is a characterization of the measured IV curve, representing how "square" the curve is, which indicates how efficiently the photogenerated carriers are extracted and transported. It is considered a ratio between the maximum achievable power, and the power generated at the V_{oc} and I_{sc}, and has a current maximum at 90%; more regularly it is between 50-70% for third generation solar cells [60]. Since the V_{oc} and J_{sc} are the major metrics defining the operating conditions for the cell, increased values are desired for high performing devices. Although the PCE and FF both define how well the cell converts photons to electrical energy, the PCE is more useful for comparisons between different kinds of SCs due to its more regular reporting across all types of solar cells. A higher PCE and FF closer to one indicate a well fabricated and high-performing cell. These four metrics are standard for the comparison between cells of different types.

2.2: Supercapacitor Working Mechanisms

Supercapacitors are an emerging energy storage system, that stores energy and allows for fast and easy charge and discharge. Unlike traditional capacitors that use dielectric materials to store energy in an electric field, supercapacitors store energy in an electrochemical form utilizing an electrolyte between two active electrodes [61]. In terms of the amount of energy and the way the energy is stored, the supercapacitor is an intermediate between dielectric capacitors and batteries. The supercapacitor has a higher power density than a battery, and higher energy density than a dielectric capacitor, although these energy density values are still lower than the current values seen in batteries [62]. Supercapacitors typically consist of two electrodes on current collectors, separated by a liquid, gel, or solid electrolyte that facilitates the energy storage [30, 61, 62]. The electrode material and the electrolyte define what type of supercapacitive mechanism is

used to store the electrochemical energy, with three major types of supercapacitor arising: electric double-layer capacitors (EDLCs), pseudocapacitors, and hybrid supercapacitors [62]. The performance of the three mechanisms are measured and compared based on the specific capacitance (areal or mass, C_{sp}), energy density (E_g), power density (P_g), and the storage efficiency of the device. The C_{sp} is a general measure of how much capacitance the material has based on the mass of the electrode (mass or gravimetric), the area of the electrode (areal) or volume of the electrode material (volumetric) [63]. The capacitance itself is a measure of the supercapacitor's ability to store energy with respect to the difference in electric potential of the plate electrodes [64]. The E_g, and P_g are important properties that are relevant to the end applications of supercapacitors. The E_g defines how much energy the device can store either gravimetrically (Wh kg^{-1}), arealy (Wh cm^{-2}), or volumetrically (Wh cm^{-3}). The P_g defines how much power can be stored or how efficiently the stored energy can be converted for use, once again measured gravimetrically (W kg^{-1}), areally (W cm^{-2}), or volumetrically (W cm^{-3}) [65]. The storage efficiency is a measure of the stability of the storage device after a number of testing cycles.

A high-performing supercapacitor will have high C_{sp}, E_g, P_g, and storage efficiency values, however, each storage mechanism will result in a different performance with better strengths [30, 31]. For example, EDLCs are likely to have the lowest power density available, while hybrid supercapacitors tend to show much higher energy and power density than the other two types, being closer to batteries [66]. Although it can be difficult to determine the functional mechanism based on these different performance metrics, and the trends do not always hold true, each of the mechanisms has different materials, and their own advantages or disadvantages that dictate their use.

The oldest and most widely used type of supercapacitor is the EDLC. The EDLC operates without a chemical or faradaic reaction, instead relying on a mechanism similar to a plate capacitor. During the charging process, as shown in Figure 5A, a potential difference is created between the two symmetrical electrodes due to an applied voltage, causing the layers to be polarized, or to gain a positive or negative charge. The ions in the electrolyte as are attracted to these layers, forming a double-layer of opposite charges at the interface of the electrode and electrolyte in Figure 5B at the fully charged state [67]. The energy is stored in this double-layer that is created during charging, depending heavily on the pore size of the electrode material, and ion concentration and size in the electrolyte [68, 69]. During discharge of the EDLC in Figure 5C, the ions are unpolarized and return to the electrolyte solution, causing a current of stored electrons to flow through the circuit [30]. Carbon-based electrodes with large pores and large active surface areas favor this mechanism, and tend to show increased storage ability as the active surface area is increased with a compatible electrolyte [14, 30, 70]. Electrolytes for EDLCs consist of free-moving anions and cations in a liquid, gel, or solid form, depending on the state of the solution in use. For this purpose, protic acids or bases like H_2SO_4, H_3PO_4, and KOH in an aqueous solution or gel, or aprotic electrolytes containing Li salts are used [14, 71].

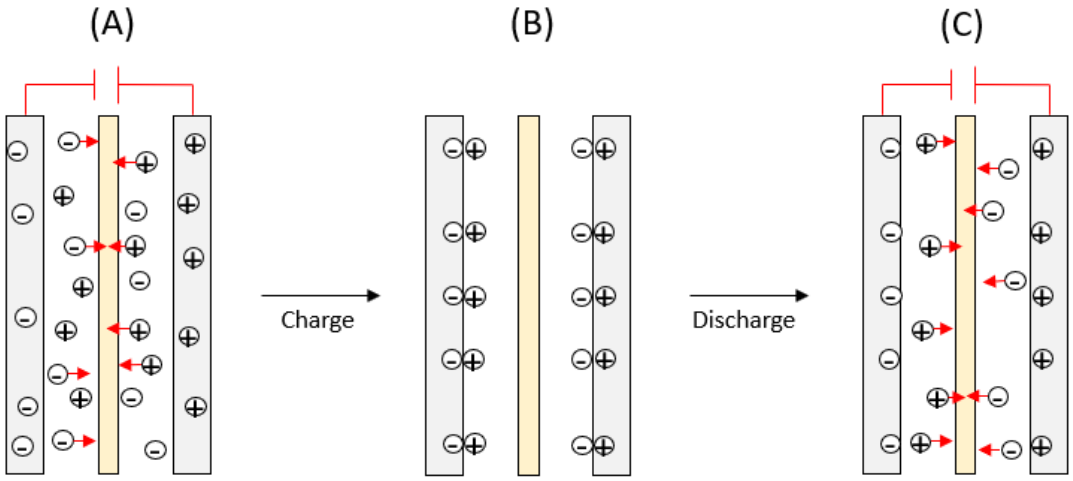

Figure 5: Operating principles of an EDLC. (A) Movement of charged ions during charge. (B) Formation of electric double-layer when the device is in the charged state. (C) Movement of charged ions during discharge, creating an electric current.

The second most widely used supercapacitor is the Pseudocapacitor. Pseudocapacitors store energy through chemical reactions know as faradic reactions, making this type more likened to ion batteries than EDLCs. Faradaic reactions are reversible oxidation/reduction reactions that cause a faradic current to flow. Three mechanisms have been defined as pseudocapacitive [72], although, as it is not the focus of this article in latter sections, only a brief overview of pseudo-capacitance will be given. For all three types, during charging, a redox reaction occurs between the electrode and electrolyte as an external voltage is applied, storing energy chemically in the products of the reaction, what type of product differs depending on the pseudocapacitive mechanism [30, 72]. During discharge, the redox reaction is reversed, releasing the stored charge as a faradic current [14, 30, 31, 68]. This mechanism is similar to the mechanism of storage in an ion battery, but occurs much faster in supercapacitors because its rate of reaction is not driven by ion mass transfer, making it non-diffusion limited [70]. It is illustrated in Figure 6. The electrode

materials for pseudocapacitors are unique because of the required faradaic reaction. Like the EDLC, the material requires high surface area and conductivity, they also need to be stable, and capable of performing reversible redox reactions with the electrolyte [73, 74]. Transition metal oxides, nitrides, and conducting polymers have been favored as pseudocapacitive materials meeting these requirements, either in symmetric or asymmetric forms [31, 72-74]. The electrolytes used in pseudocapacitors depends heavily on the electrode materials chosen, but there are some common types; Na_2SO_4, group I hydroxides, and several acids in aqueous or non-aqueous solutions have been used in several studies [71, 74].

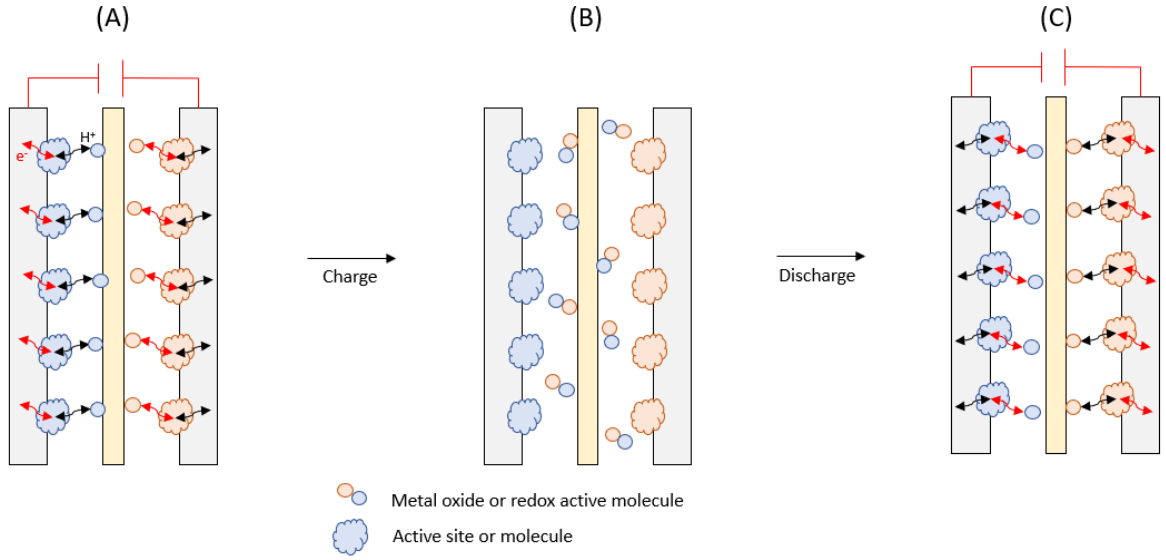

Figure 6: Operating Principles of a Pseudocapacitor. (A) Redox reaction occurring between the active sites on the electrode and the electrolyte during charging. (B) Formation of metal oxide or redox active molecule after charging. (C) Reverse redox reaction generating a faradaic current during discharge.

The final type of supercapacitor uses the hybrid mechanism for energy storage. This supercapacitor is still in the research and development stage, but is being used increasingly often due to their desirable properties and their ability to bridge the gap between the other two

supercapacitor types and their performance which is nearest to batteries [14, 75]. Unlike EDLCs and the pseudocapacitor mechanism, hybrid supercapacitors require asymmetric electrodes to achieve their mechanism, which is a mix of double-layers and pseudo-capacitance, each individual mechanism taking place at a different electrode, as defined in Figure 7 [66]. During the charging process, a redox reaction occurs at the anode, storing energy using the pseudocapacitive mechanism such as illustrated in Figure 7A. An electric double-layer forms at the cathode of the device, storing energy with the EDLC mechanism as a voltage is applied. When fully charged and no longer receiving an input as in Figure 7B, an electric double layer is formed at the EDLC, and the redox reaction ceases. When discharging as in Figure 7C, the redox reaction is reversed at the anode, and the double-layer is dispersed, creating a faradaic current in the circuit. The main benefit of this mechanism is a high current driven by both the faradic process and the electric double-layer, avoiding the drawbacks of each type and achieving improved energy and power density over the other two types of supercapacitor, although at the cost of lower cyclability [30, 66]. The performance of this type of supercapacitor depends on the electrodes and electrolytes chosen for the device, which leads to the largest challenge for this device: determining compatible materials [31, 68]. The most standard combination of electrodes is an asymmetric system with a carbon-based electrode, and a metal-oxide or pseudocapacitive electrode [31, 66, 71]. The possible electrolytes that can be used for this type of device encompass all the liquid, gel, and solid materials that are used for EDLCs and Pseudocapacitors and are compatible with the electrodes chosen [71].

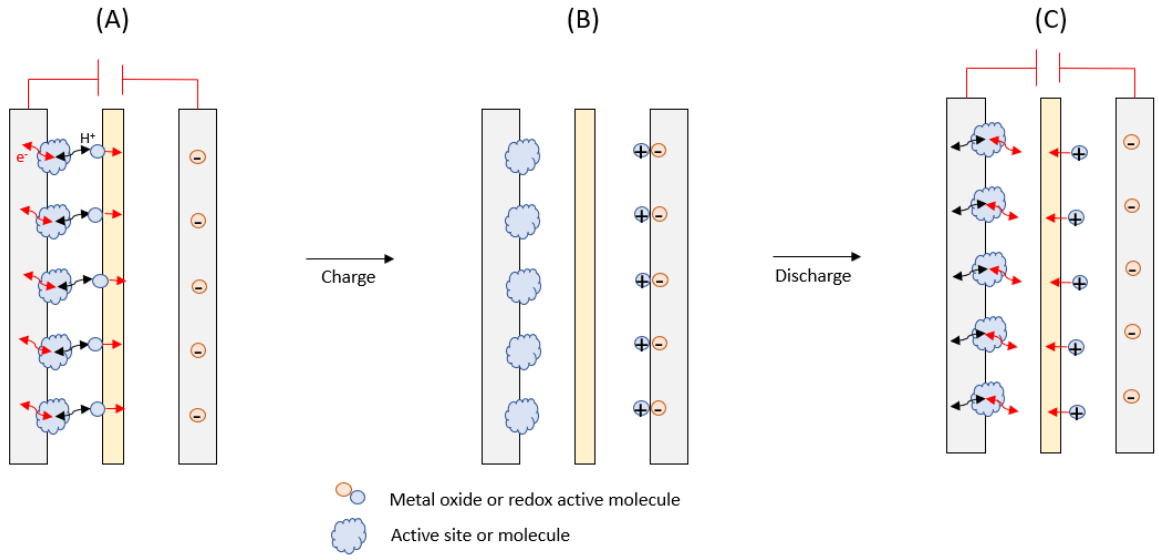

Figure 7: Operating principles of a hybrid supercapacitor. (A) A redox reaction takes place between the anode and the electrolyte, yielding charged ions that are attracted to the opposite charge during charging. (B) The device is at equilibrium after charging with the cathode hosting a double-layer. (C) The double-layer is released, and the redox reaction is reversed during discharge.

2.3: Integrated Devices

The most desirable structure for an integrated solar cell and supercapacitor device has high safety, cost effective manufacture, and high efficiency. Separated or strictly modular devices connected by external wires cannot fulfill these qualifications and tend to suffer from further issues like complex design and packaging to account for the wiring, making them unportable [76]. It is possible to reduce the portability issues by developing an all-in-one or monolithic structure. In these structures, power generated by the SC is transferred directly to the supercapacitor within the same device instead of travelling to an external module. This has the benefit of compensating for the natural power fluctuation of the solar cell due to changing conditions, quick charge times for

the supercapacitor module, and the ability of the system to operate as a backup power source in times of low light [77, 78]. Such monolithic devices incorporating the energy generation and energy storage modules can further separated by their overarching configuration, two-electrode, and three-electrode devices, both of which can be further modified into various architecture. Changing the overarching configuration can alter the integral properties of the device that determine the overall efficiency, such as the operating voltage, operating photocurrent, energy conversion and storage mechanism, and the internal resistance [79]. The choice of configuration and architecture depends on the materials utilized, the desired properties, such as operating voltage or current, and the geometry of completed device.

2.3.1: Two-Electrode Device Configurations

The two-electrode configuration changes the mechanisms of energy conversion and storage, as well as the device geometry. Two architectures exist for this type of device: a monolithic structure that contains a thin, porous layer separating the DSSC and supercapacitor, or a direct two-electrode DSSC that also stores energy by an internal mechanism [79, 80]. The monolithic architecture illustrated in Figure 8A is the oldest layout defined for this type of integrated device and operates with a well understood mechanism. This device uses the natural charge separation that occurs upon the movement of excited electrons into the conduction band to begin the charge process. After the conversion of photons to electrical energy in the DSSC through charge separation, the electrons are transferred to the load and then to the CE, where the charge accumulates. A positive and negative charge is generated on either of the supercapacitor electrodes, one of which is a porous layer between the DSSC photoanode and the supercapacitor electrolyte, creating an electric double-layer storage mechanism. The EDLC mechanism is the easiest to achieve with this architecture based on the constraints in the number of electrodes and

the most common materials used with this layout, making the entire device a photo-driven capacitor [34].

A direct two-electrode device does not include the thin, porous layer that segregates the DSSC and supercapacitor as in the monolithic devices. Due to the absence of the thin layer like is illustrated in Figure 8B, this architecture is less efficient in both conversion and storage than the individual modules alone. Charge recombination and electrolyte incompatibility are the reasons for the inefficiency, which are the largest issues delaying the development of these devices [80, 81]. The energy conversion mechanism for this architecture is principally the same as a traditional DSSC. The storage mechanism for this architecture is most often the creation of a double-layer of separated charges at the photoanode with a focus on avoiding recombination when not actively charging the device. Effectively, the storage mechanism functions like a hybrid supercapacitor, where the separated charge from the photoanode is accumulated in a double-layer on the counter electrode surface and rest of the energy is stored by the faradaic reaction taking place to result in the separated charges. The accumulated charges appears either on the modified CE alone, or on both the photoanode and the CE of the DSSC [80, 82, 83]. On discharge, the stored charge in the form of the hybrid electric double-layer is released to the external load as if the DSSC was still receiving light until the stored energy is depleted [80, 84]. For this type, avoiding recombination while not actively charging the device is the most important element for further development, because that will improve the storage capabilities and ultimate performance [80]. Additionally, determining an electrolyte that can fulfill both the energy storage and conversion processes efficiently is paramount [85-87].

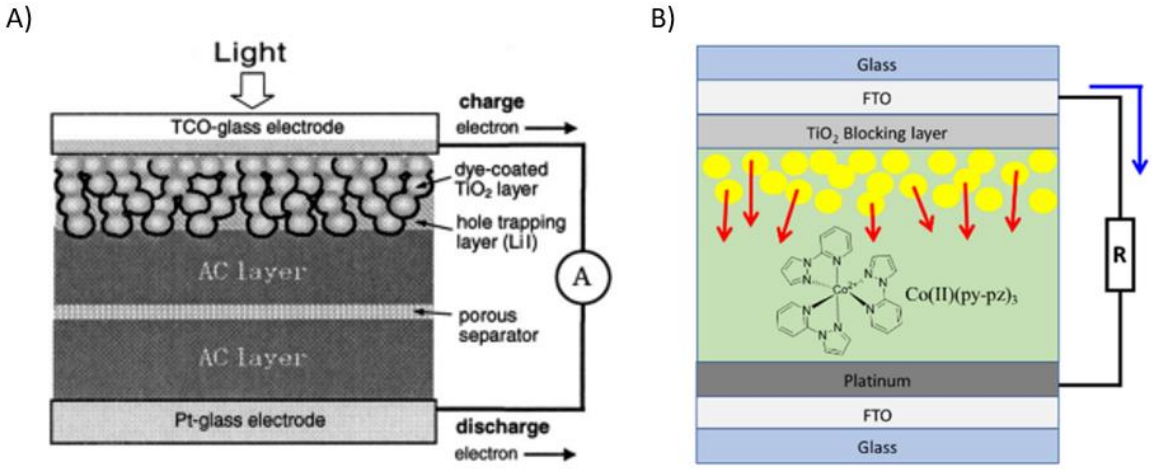

Figure 8: Structure of two-electrode integrated devices. (A) Two-electrode monolithic device using AC as an EDLC [34]. (B) Two-electrode direct device. Reprinted with permission from [80]. Copyright 2023 American Chemical Society.

2.3.2: Two-electrode Devices

Numerous two-electrode devices have been fabricated in the years since this structure was initially developed. This section will introduce some of the major break throughs in both the monolithic and direct architecture, and some notable cells that have been developed.

Miyasaka et al. fabricated the first notable rigid, monolithic, two-electrode integrated device utilizing a Dye-Sensitized Solar Cell and supercapacitor (DSSCSC). The photocapacitor was prepared with nanocrystalline TiO_2 particles doctor-bladed onto an FTO slide, then sensitized by the absorption of a Ru complex dye. A liquid suspension consisting of Activated Carbon (AC), poly-vinylflouride, and N,N-dimethylformamide was cast and dried on the sensitized film, which was then enclosed by the counter-electrode of Pt-coated glass, also covered with a film of Activated Carbon. The remaining gap between the two electrodes was filled with an electrolyte solution. The resulting device showed good cyclability, with a Coulombic efficiency ranging from

59% initially to 80% in later cycles, and a capacitance of 0.69 F cm^{-2} [34]. Overall, this monolithic two-electrode system acted as a proof-of-concept for the integration of the two devices, helped highlight the inherent problems that can arise in this structure, and paved the way for further investigations.

Kulesza et al. compared a monolithic two-electrode device to a monolithic three electrode device in order to show the performance difference more directly. The two-electrode device consisting of an N719 dye-activated TiO_2 photoanode with an iodide/triiodide electrolyte in contact with an internal supercapacitor. The supercapacitor included symmetric PEDOT/CNT electrodes separated by a $LiCF_3SO_3$/PC electrolyte. The three-electrode device had the structure, in order from the transparent current collector, of FTO/TiO_2/D35 (photoelectrode) + P3HT/Ag/$RuO_x(OH)_y$ + Nafion™ (separator and electrolyte) + $RuO_x(OH)_y$/FTO, where the P3HT/Ag/$RuO_x(OH)_y$ segment acted as a dual-sided intermediate electrode. The devices showed large differences in coulombic efficiency at 7.8% and 87.8% for the two- and three-electrode, respectively. The efficiency difference was attributed to the Ag intermediate electrode reducing the ohmic drops occurring during charging/discharging, disallowed the movement of the SC electrolyte into the storage section. Its dual performance as a current collector and electron and hole transporter further proved the better performance of the three-electrode system [36].

Although this comparison shows a vast improvement in the performance of the three-electrode device in comparison, the monolithic two-electrode device can still be made functional with the use of spacers and sealants that fix the various issues that arise with the leakage of the electrolyte and high internal resistance. One example of a monolithic two-electrode device used a sulfur-based redox electrolyte and a multi-walled carbon nanotube (MWCNT) supercapacitor module in order to create an integrated cell that was high performing and flexible, unlike many

previous examples. The device had a high PCE of 6.1%, a mass C_{sp} at 48 F g^{-1}, and a storage efficiency at 84%, proving that it is possible for this architecture to avoid leakages and improve performance although balancing PCE and high C_{sp} is difficult with this type of integrated device [88].

Direct two-electrode devices are much rarer in comparison to the monolithic structure due to their drawbacks regarding longevity, with only a few notable examples having been tested [80-83, 89]. Zhang et al. developed the earliest examples of this structure testing a traditional TiO_2 DSSC merged with a modified Pt-coated PVDF/zinc nanowire array (ZNWA) CE in 2013. The conversion and charging mechanism for this device operated as a typical DSSC that transferred separated electrons to the modified CE. The electrons created an electric double-layer on the ZNWA and the surface of the Pt. This device achieved a PCE of 3.70% on average and an energy density of 1.4 mW-h kg^{-1}, the low values were attributed to the recombination of separated charges in the cell [82].

Yilmaz et al. also fabricated a direct two-electrode device utilizing N719-sensitized TiO2 on an FTO glass substrate as the DSSC, fabricated by the traditional doctor-blading method, and MnO_2 coated micro-array Carbon nanotubes (MACNTs) as the supercapacitor, fabricated through electrochemical deposition. The dual electrolyte consisted of 1M TEABF4 in acetonitrile with the active redox couple BF^{4-}/BF^{3-} that was saturated on both electrode surfaces before they were combined into one device. The device was characterized using galvanostatic-discharge and I-V measurements under 1 sun illumination. The best results of the I-V measurements showed an Isc of 0.749 mA/cm2, a Voc of 0.46 V, and a maximum fill factor of 19.3%. The highest charging potential and capacitance of the device were 0.955 V and 13.1 mF cm^{-2} respectively, achieved at a discharge current of 10 µA after 40 minutes of charging under 1 sun illumination. The cyclability

and performance efficiency was not reported, and the overall low performance of the cell was attributed to the TEABF4 electrolyte, which could only support a single electron transfer [81].

Two major examples of this structure converted the DSSC to a photo-capacitor without modifying the device to have capacitor specific electrodes. The mechanism for the device relied on the formation of double-layers during the photon conversion process in DSSCs and stored the energy by suppressing the charge recombination. The first device was modified from a traditional DSSC by reducing the number of oxidizing centers in the Co(II)(py-pz)$_3$ complex in 3-methoxypropionitrile electrolyte. The result was a stable cell that retained its charge in the dark after 32 cycles and an areal C_{sp} of 1.4 mF cm^{-2} [80]. More recently a group modified the sensitizers present in the cell to absorb light in a wide range such as white light and near infrared. The best performing organic sensitizer was based on chromophores, labelled LF15 by the group, having a wide absorption band, a higher degree of dye absorption, and the highest J_{sc} at 2.14±0.60 mA cm^{-2} under white light and 1.85 mA cm^{-2} near infrared. The cells were all very stable over 50 charging/discharging cycles, showing little loss in V_{oc} as the cycles progressed. The areal C_{sp} depended on the light source and dye loading, the LF15 dye, performed well with a C_{sp} of 2.58±0.11 mF cm^{-2} under a white LED, and 2.48±0.17 mF cm^{-2} under near-infrared conditions at a wavelength of 740 nm [89].

Although desirable for their simple fabrication and materials that could save on development and manufacturing costs, the performance of the two-electrode devices is not high in comparison to the three electrode devices that are the larger focus of this thesis and discussed at length in sections 2.3.3 through 2.3.4.

2.3.3: Three-electrode Device Configurations

A three-electrode device introduces a degree of separation between the two modules by the addition of a common or intermediate electrode. One side or portion of the intermediate electrode (IE) acts as part of the SC, and the other side acts as part of the supercapacitor [35]. This configuration is also split into two separate architectures that are similar in their fundamental mechanisms: monolithic structures and the shared-substrate architecture. Devices with the monolithic architecture – shown in Figure 9A – use an IE as previously stated, typically for this architecture, it is double-sided with similar or different materials coated onto a conductive substrate [28, 35, 79]. For this type of device, the charging and conversion processes take place at the same time and can be used as if they were separate devices. The creation of electron-hole pairs causes a separation of charge in the photovoltaic layer, and electrons are transferred to the back contact, which prompts the storage mechanism. A separation of charge also accumulates on the IE, which can be collected in the energy storage module, or used to power an external load [15, 90]. During discharge, the DSSC module is disconnected, and the supercapacitor module is connected to the external load via the IE, which releases the stored energy in a mechanism dependent on the supercapacitor type that was fabricated [28]. Compared to the two-electrode monolithic device, this complex architecture lessens the amount of internal resistance that occurs due to the shared electrolyte that is present in both types of two-electrode devices, thereby improving the energy conversion and storage capabilities of the device [35].

Growing more common, the three-electrode, shared-substrate architecture typically connects the energy harvesting and storage module in series or in parallel through a transparent conductive substrate or current collector that functions as the IE between the modules, making the device thinner overall as outlined in Figure 9B [91, 92]. The current collector for this architecture

determines the flexibility of the overall device, either being a rigid transparent conductive oxide, or a flexible conductive polymer. Fundamentally, regardless of the device flexibility due to the substrate, the charging and discharging mechanisms for the shared substrate device is similar to the monolithic architecture because the current collector functions as the IE. The largest difference being the placement of the modules in comparison to the other, side-by-side on the same plane rather than stacked monolithically [93, 94]. Compared to the traditional monolithic architecture, these devices can have increased stability and simplicity in fabrication due to the lack of a sandwich structure that is present in the monolithic devices, making it uncomplicated to keep the DSSC and supercapacitor electrolytes separate, and reducing errors that can arise due to that issue [95, 96].

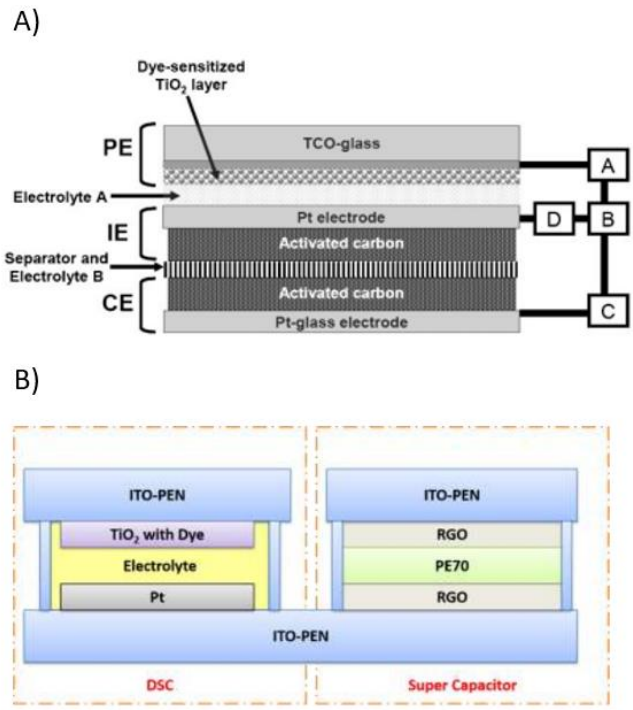

Figure 9: Structure of three-electrode integrated devices. (A) Three-electrode monolithic device with an intermediate electrode made of Pt [35]. (B) Three-electrode shared substrate device with the conductive substrate acting as the intermediate electrode [93].

2.3.4: Three-Electrode Devices

Three-electrode devices were developed to directly address the issues noticed in the first two-electrode device fabricated by Miyasaka [34]. The first three-electrode device differed from the previous two-electrode iteration by the inclusion of a Pt IE between the DSSC and the EDLC. This inclusion served to improve the charging voltage to 0.8 V and the E_g to 47 μW-h cm^{-2}, reducing the occurrence of charge recombination, the internal resistance, and the chance of a short circuit from electrolyte leakage [35]. These devices can also be made easily flexible by the inclusion of flexible substrates and intermediate electrodes, with no difference in mechanism. A summary of the comparable studies, using the monolithic and shared-substrate (SS) architectures under standard conditions of 1 Sun or 100 mW cm^{-2} unless otherwise specified, is shown in Table 1.

Generally, there has been some consistency in the materials used for the components of the integrated cells, like the consistent usage of TiO_2 as the photoanodic material, or synthetic dyes. Improvements to the cell have included changing the supercapacitor type, changing the electrodes for both modules, changing the IE material, changing the electrolytes, or a combination of the four. Some cases showed little forward growth with poor performance and are thus not included in the tables [97-99]. Other included cases [100, 101] were not integrated devices, but utilized identical or similar materials to fabricate both a DSSC and a supercapacitor as separate devices, demonstrating promising capabilities with both devices that could be integrated in the future. Integrating these devices into one cell is a potential area of future study.

The most recent studies regarding integrated devices over the last few years have focused on determining highly effective electrodes that function well for both the DSSC and supercapacitor modules, and mixing materials for truly bifunctional electrodes [102, 103]. One recent group

modified the electrodes by doping in order to obtain high-performing/low-cost materials. The bifunctional electrode in this case consisted of Boron-doped carbon-fiber manufactured with electrospinning and coated on a Ti foil IE. The integrated monolithic device manufactured with these materials saw a C_{sp} at 41.2 g^{-1}, and an overall conversion and storage efficiency of 1.19%, higher than the 0.7% overall efficiency that was achieved with the non-doped carbon-fibers [103]. Alternative studies mix the electrode materials to obtain the best performance, for example, a shared substrate architecture that uses FTO as the IE, coated with Pt as the CE for the DSSC, and a Co-based material for the supercapacitor module. The resulting integrated device was highly stable and high performing, with a PCE of 6.3% with the Pt CE, and a C_{sp} of 385 F g^{-1} with a symmetric CoSbS/MWCNT supercapacitor [102].

Beyond simply changing components, other studies used multiple modules in combination to create a single high-performance cell. For example, Scalia et al. fabricated a monolithic three-electrode device with four DSSCs connected to a single large area supercapacitor as illustrated in Figure 10A for an increased output voltage relating to the V_{oc} as seen in Table 1 [104]. Of the published devices that are included in the table, the best performance was achieved by Maddala's group, with a cell in the shared-substrate architecture, using FTO as the current collector. Unlike Scalia et al, who connected four DSSC cells on the same plane to the monolithic supercapacitor [25, 104], the resulting device connected six DSSCs as shown in Figure 10B to one supercapacitor on the same plane, resulting in a high V_{oc}, PCE, and overall device efficiency, implying that a higher output voltage and PCE in the DSSC module, paired with a compatible supercapacitor, can increase the efficiency of the combined cell dramatically [94].

TABLE 1

THREE-ELECTRODE DSSC-SUPERCAPACITOR DEVICES

DSSC				Both	Supercapacitor				
Electrolyte/HTM	CE	V_{oc} (V)	PCE	IE	Electrode	Electrolyte	C_{sp}	η	Reference
I^-/I^{3-}	AC	0.82	---	Pt	AC	TEATFB/PC	0.65 F cm^{-2}	---	[35]
I^-/I^{3-}	Pt	0.75	---	Pt	PProDOT-Et_2	---	6.5 F cm^{-2}	0.60%	[105]
I^-/I^{3-}	Pt	0.42	---	Ti	TiO_2 array	ZrO_2 (separator)	140 μF cm^{-2}	----	[106]
P3HT	P3HT	0.898	2-3%	Ag	$RuO_x(OH)_y$	Nafion™	370 F g^{-1}	--	[107]
P3HT	P3HT	0.9	0.001%	Ag	$RuO_x(OH)_y$	Nafion™	3.26 F cm^{-2}	---	[36]
I^-/I^{3-}	MWCNT	0.75	6.10%	MWCNT	MWCNT	PVA/H_3PO_4	26 F g^{-1}	5.12%	[88]
I^-/I^{3-}	MWCNT-PANI	0.75	6.10%	MWCNT-PANI	MWCNT-PANI	PVA/H_3PO_4	208 F g^{-1}	4.29%	[88]
Co^{-2}/Co^{-3}	PDOT	0.8	4.90%	Ni Foil	Ni(Co)O/AC (Asymmetric)	KOH	46 F g^{-1}	0.60%	[108]
I^-/I^{3-}	Pt	0.63	3.17%	Ti	TiO_2 array	Li_2SO_4	1.289 mF cm^{-2}	1.64%	[109]
I^-/I^{3-}	Si wafer	0.68	4.80%	Si Wafer	Si Wafer	PEO/EMIBF4	3.5 mF cm^{-2}	2.10%	[110]
I^-/I^{3-}	Ppy/rGO	1	2.40%	Graphite	Ppy/rGO	PVA/KOH	308.1 F g^{-1}	---	[111]
I^-/I^{3-}	Pt	2.57	2.25%	Meltonix Film	AC	PEO:Pyr14TFSI	9 mF cm^{-2}	1.67%	[104]
I^-/I^{3-}	SCS	0.791	6.69%	---	Solid carbon sphere (CSC)	KOH	124.9 F g^{-1}	---	[100]
I^-/I^{3-}	NCS	0.804	8.64%	---	N-doped carbon sphere (NCS)	KOH	224.6 F g^{-1}	---	[100]
PVA-PVP-TBAI	rGO	0.5	1.06%	FTO	rGO	PVA-PVP/TBAI	1.327 F g^{-1}	---	[112]
I^-/I^{3-}	SWCNH	0.72	11.12%	FTO	SWCNH	EMIBF4	---	---	[94]
I^-/I^{3-}	SWCNH	3.94	19.71%	FTO	SWCNH	EMIBF4	74.27 F g^{-1}	10.46%	[94]
I^-/I^{3-} gel	$FeCo_2O_4$	0.75	6.04%	---	$FeCo_2O_4$/rGO (Asymmetric)	PVA/KOH	93.8 F g^{-1}	---	[101]
---	BCf	0.78	7.51%	Ti Foil	BCf	Li_2SO_4	41.2 F g^{-1}	1.19%	[103]
I^-/I^{3-}	Pt	0.84	6.3%	FTO	CoSbS/MWCNT	Na_2SO_4	382 F g^{-1}	---	[102]

TABLE 2 (continued)

THREE-ELECTRODE DSSC-SUPERCAPACITOR DEVICES

s	Architecture	Dye
	Monolithic	N719
	Monolithic	N3
	Monolithic	Eosin Gelblich
	Monolithic	D35
	Monolithic	D35
	Monolithic	N719
	Monolithic	N719
	Monolithic	LEG 4
	Monolithic	N749
	Monolithic	N719
	Monolithic	N3
	Monolithic	Z907
	Not Integrated	N719
	Not Integrated	N719
	SS	CaBa
	SS (x1 cell)	N719
	SS (x6 cells)	N719
	Not Integrated	N719
	Monolithic	N719
	SS	N719

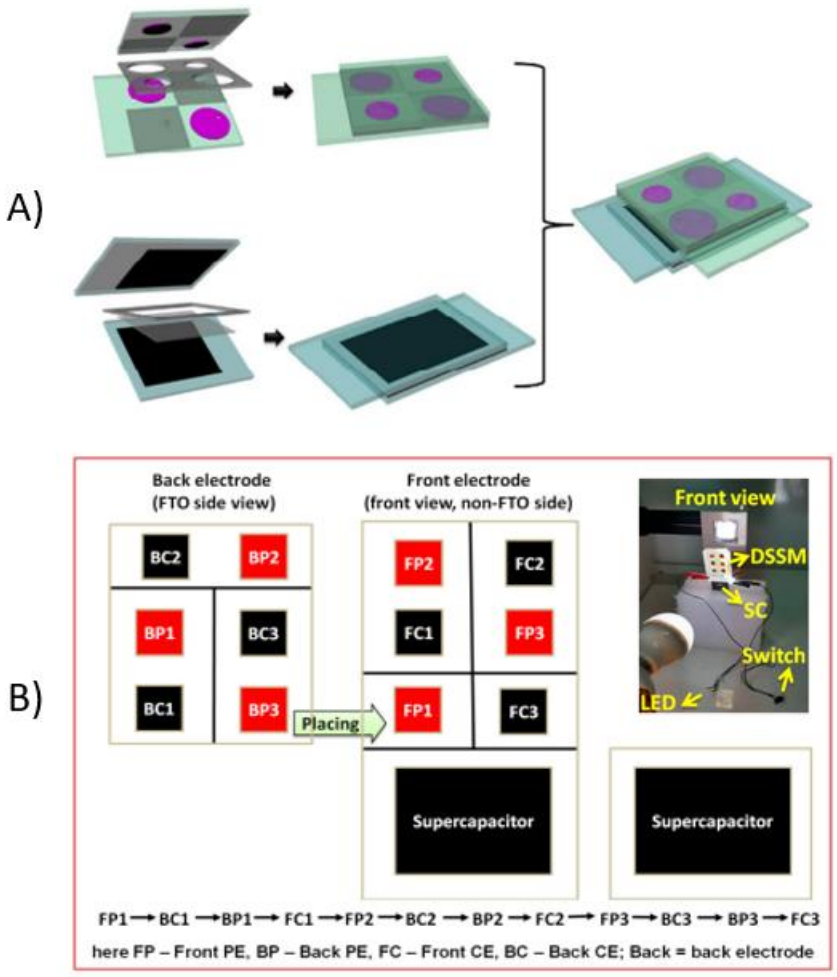

Figure 10: Three-electrode devices with multiple DSSC modules. (A) Monolithic three-electrode device with four DSSCs in one module and one large area EDLC [25]. (B) Shared Substrate device with 6 DSSC, connected to one large area supercapacitor. Inset: the completed device undergoing photocharging from two sides. Reprinted with permission from [94]. Copyright 2023 American Chemical Society.

Further devices that were not included in the table are still considered three-electrode devices but use novel materials and architectural designs to modify the performance from the basic designs. One such study attempts to bridge the two electrode and three electrode configurations

with a modified bifunctional electrolyte. The bifunctional electrolyte consisted of a three sections, two modified for DSSC and supercapacitor use, and a center section that acted as an impermeable barrier to prevent electrolyte leakage and simplify manufacture, demonstrated in Figure 11A. The EDLC module for the device had high efficiency and cyclability. The DSSC for the structure had a moderate performance in comparison to modern breakthroughs, at only 4.33% PCE, which was attributed to high series resistance and imperfect interfacial contact with the electrode. The overall photo-electrical conversion and storage efficiency for the device had a maximum value of 3.72% in the first seconds of charge and decreased throughout its usage exponentially. The team concluded that although the efficiency was low, it was comparable to two- and three-electrode structures at the time, and that this in-between system could see use due to its low cost, easy manufacture, and scalability compared to three-electrode devices [85].

Other novel examples have further combined rigid and flexible substrates into singular devices in the shared substrate form to be used with more complex geometries. The study utilized a length of conductive carbon fabric as the IE, TiO_2/CdS/Rose Bengal dye as the photoanode, a S/S^2 gel-electrolyte, and PAAQ/CoTe CE as the highly modified DSSC module. The supercapacitor module consisted of symmetric PAAQ electrodes with a lithium ion conducting gel as the electrolyte and a separator, acting as a pseudocapacitor. Several configurations of the noted materials were tested, the final layout illustrated in Figure 11B with the outlined structure achieving the best PCE of 8.25% in the DSSC module. The integrated device was also well performing: the storage efficiency was 56.7%, and the overall conversion and storage efficiency was 4.68% [113]. Moving forward, the best areas of research will focus on determining high-performance, low-cost materials and layouts that increase the performance of integrated devices while remaining safe and efficient.

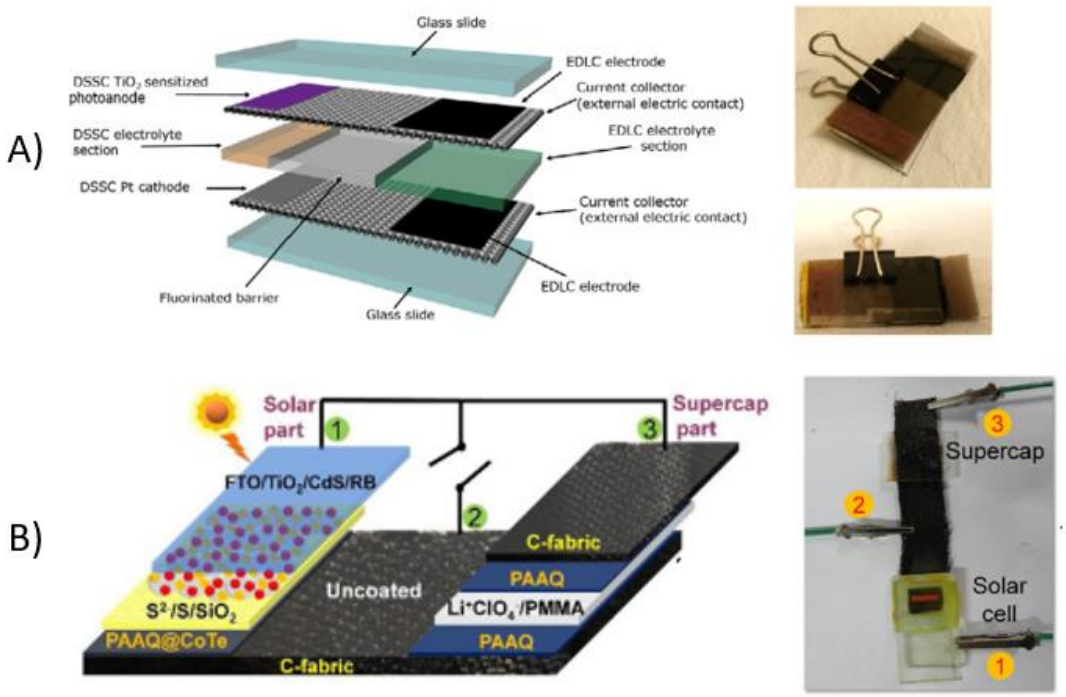

Figure 11: Novel modifications to the three-electrode configuration. (A) Shared Substrate type device with bifunctional electrolyte, bridging the gap between two-electrode and three-electrode devices. Inset: the completed device [85]. (B) Structure of a shared substrate device with C-fabric as the IE. Inset: the completed device [113].

2.3.5: Alterative Devices and Configurations

Integrated devices have also been made into fibrous devices intended to be highly flexible in form and in applications. It is desired due to the increasing reliance on portable electronics. Fabricating such high-performance energy systems in a compact, one-dimensional fibrous structure can relieve limitation in heavier and bulkier traditional panel structures [114]. The small and lightweight design is good for an increasingly large number of applications, like comfortable medical sensors, wearable power packs, and any other field where the comfort and mobility of the user are paramount [84, 115]. To properly construct such wearable devices, the fiber electrodes

must be able to bend, stretch, and twist while still retaining electrical conductivity, efficiency, and mechanical properties [116]. Since DSSCs are often inexpensive, and easily fabricated with a wide range of photoanodes, electrolytes, and CEs, they can easily achieve the flexibility necessary for fibers, which emerged as early as 2005 in a coaxial, or centralized along-the-fiber, architecture [27, 117, 118]. These devices are separated in coaxial, twisted, and parallel architectures, displayed in Figure 12, which define how the devices layout the DSSC and supercapacitor in regard to the other two types [79, 119].

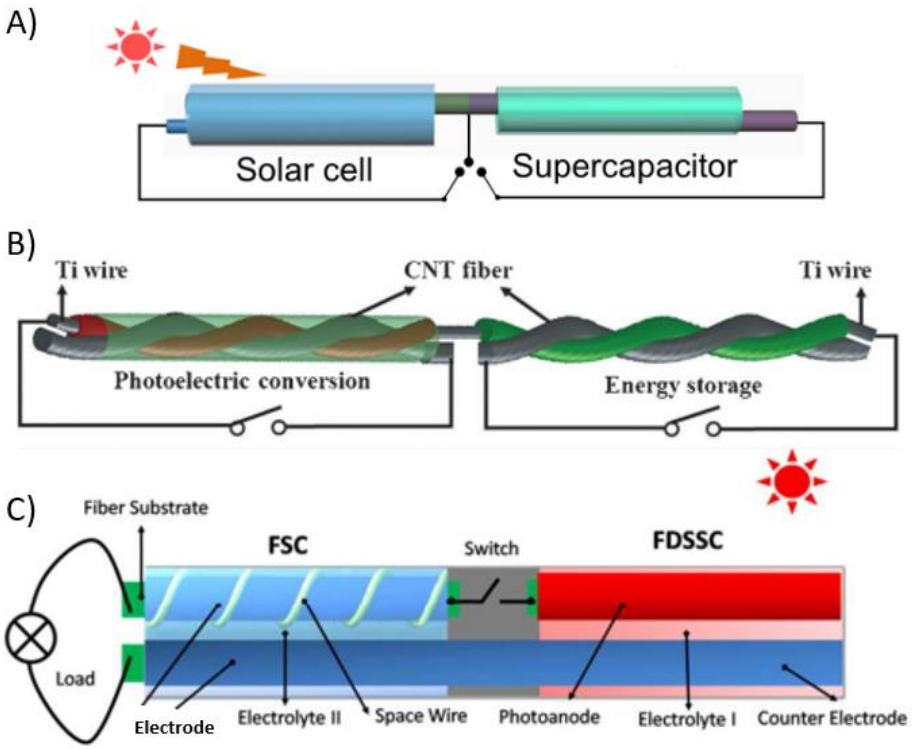

Figure 12: Fibrous DSSC-Supercapacitor Configurations. (A) Coaxial fibrous DSSCSC where both devices lie along the same, multifunctional fiber [120]. (B) Twisted fibrous DSSCSC where the devices are twisted to form a single fiber textile [121]. (C) Parallel fibrous DSSCSC where the two modules share a common fiber-electrode and have separate, function specific parallel electrodes [78].

Bae at al. made the first fiber DSSCSC from a coaxial nanogenerator, DSSC, and supercapacitor in 2011. ZnO nanowires are the active electrodes, a thin Au layer is the shared electrode on the PMMA micro-fiber substrate in the structures, allowing for graphene-coated Cu-mesh to be used as the external electrodes for all three units on the coaxial fiber. The DSSC module contained a liquid dye and electrolyte, ultimately showing a poor PCE of 0.02%, attributed mainly to the transparency of the external Cu-mesh. This problem would be fixed in subsequent cases.

The asymmetric supercapacitor utilized the same external electrode as the DSSC, with the inclusion of a gel-type PVA-H_3PO_4 electrolyte, reporting a capacitance per unit length of 0.025 mF cm^{-1} [114]. From this point, the capabilities of fibrous DSSCSCs would generally trend upward, as seen in Table 2, with some notable recent trends.

TABLE 3

FIBROUS DSSC-SUPERCAPACITOR DEVICES

DSSC			Supercapacitor					
V_{oc} (V)	PCE	CE	Axial Electrode	Electrode	Electrolyte	C_{sp}	$\eta_{overall}$	Reference
0.17	0.02%	Graphene /Cu-mesh	PMMA/Au/ZnO	ZnO/Graphene (Asymmetric)	PVA-H_3PO_4	0.4 mF cm^{-2}	---	[114]
0.68	2.20%	CNT	Ti Wire	CNT (Asymmetric)	PVA-H_3PO_4	0.6 mF cm^{-2}	1.50%	[121]
0.622	4.56%	PANI-SS	PANI-SS/Pt	PANI-SS	H_2SO_4	19 mF cm^{-2}	2.10%	[78]
---	6.58%	PANI-CNT	Ti Wire/CNT	PANI/CNT	Li^+ ions	2.13 mF cm^{-2}	---	[122]
0.635	2.73%	CNT	Ti Wire	CNT	PVA-H_3PO_4	3.32 mF cm^{-2}	1.20%	[123]
0.68	6.47%	CNT	Ti Wire/CNT	CNT	PVA-H_3PO_4	21.7 F g^{-1}	1.83%	[124]
0.74	9.50%	CF/TiO_2/MoS_2	CF	CF/TiO_2/MoS_2	PVA-H_3PO_4	18.51 mF cm^{-2}	---	[125]
---	4.73%	Pt on PANI@G	PANI/Pt@G on Cu	PANI//Pt@G	---	284 mF cm^{-2}	3.07%	[120]
0.74	7.30%	PEDOT-MA	PEDOT-MS	PEDOT-MS	LiCl-PVA	251.2 mF cm^{-2}	5.10%	[126]
0.6	4.20%	G/CNT/PANI	G/CNT/PANI	G/CNT/PANI	PVA-H_3PO_4	472 mF cm^{-2}	2.10%	[127]
0.745	7.99%	---	PEDOT:PSS	PEDOT:PSS	---	---	4.2%	[128]

TABLE 4 (continued)

FIBROUS DSSC-SUPERCAPACITOR DEVICES

s	Configuration	Coaxial	Twisted	Parallel	Twisted	Coaxial	Coaxial/Twisted	Parallel	Coaxial	Parallel	Parallel	Coaxial

Fibrous DSSCs have shown more definite linear improvement than rigid structures, with some small exceptions to the rule using different configurations. The electrolyte and dye columns were omitted because all cases utilized uniform I^-/I^{-3} redox reaction electrolytes and N719 for the dye. The results also typically use the same TiO_2 based photoanodic material, excluding the first entry in the table, which used ZnO [114]. The parallel configuration seems to currently offer the most consistent performance for integrated cells, reaching an overall peak efficiency of 5.10%, although the highest PCE has been achieved with a coaxial hollow-composite fiber that is fully bifunctional without further modification [128, 129]. Future considerations for this structure type should likely consider further improvements in the individual devices and determine how they can either be integrated coaxially for space saving and durable fibers, or if parallel fibers will still prove to have the highest photovoltaic performance going forward.

Alternative devices have also been made with a range of different cell types. Silicon solar cells have been combined with batteries to commercial success, and with supercapacitors to a lesser extent [9, 130, 131]. Third generation solar cells like perovskite SCs, organics SCs, and quantum dot-sensitized SCs have also been fabricated with batteries and supercapacitors using the previously defined configurations. The performance results of these alternative devices have been collated in a number of different reviews [10, 15, 43, 79, 84, 132-136].

CHAPTER 3

EXPERIMENTAL

3.1: Materials

The photo-electrode used in this work consisted of Titanium (IV) Oxide (21nm, ≥99.5% trace metals). The sensitizing dye used in this work was cis-Bis(isothiocyanto)bis(2,2'-bipyridyl-4,4'-dicarboxylato ruthenium(II)) or N3 dye. The electrode materials included Activated Carbon (AC) powder, Mesoporous Carbon (MC) nano-powder (<500 nm particle size, 99.95%), Graphene powder (conductivity > 103 S/m), and Graphite powder (< 20 µm, synthetic). These four commercial carbon-based particulates were used as-is for counter-electrode materials, applied in the solvent 2-Propanol (> 99.5%).

The DSSC electrolyte consisted of I_2 (Iodine), Lithium Iodine (LiI), Tert-butyl-pyridine, 1-butyl-3-methylinidazolium, guanidine thiocyanate, Valenonitrile, and Acetonitrile, which were purchased and used as is, also from Sigma-Aldrich.

Poly(vinyl alcohol) (PVA) (Mw 89,000-98,000, 99+% hydrolyzed), Potassium Hydroxide (KOH) pellets (> 85%), and Glycerin (> 99.5%) were used to fabricate the supercapacitor gel-electrolyte and separator. The photoelectrode materials, four commercial carbon-based particulates, DSSC components, and EDLC electrode and separator were all purchased from Sigma Aldrich.

Also obtained were Graphite paper sheets (210 mm x 200 mm x 0.3 mm, 3mΩ/cm^2 electrical resistivity) purchased from MSE Supplies, and Fluorine-doped tin oxide (FTO) slides purchased from Hartford Glass Company (Hartford, IN), used as conductive substrate materials.

3.2: Fabrication of Dye-Sensitized Solar Cell

The photoanode was prepared by cleaning the FTO conductive slide with ethanol. A further area of 0.5 cm by 0.5 cm was demarcated by tape on the conductive surface. A TiO_2 paste was created by suspending 0.200 g TiO_2 powder in 2 mL of ethanol in a 10-20 mL glass beaker. The mixture was stirred with a glass stirring rod until homogenous. The prepared paste was applied to the demarcated area on the FTO slide by the doctor blading method, resulting in a thin even surface, that was repeated 2-3 times until a consistent thin layer was achieved on each slide. The tape was removed, and the TiO_2 layer was sintered in a box furnace, held at 500°C for 40 minutes, with a heating rate of 10°C/min. The N3 dye mixture was created in a petri dish with 0.008g of N3 dye powder, suspended in 25 mL of ethanol, and stirred with a glass stirring rod. Following sintering, the TiO_2 coated slides were dipped into the solution and allowed to sit for 24 hours.

The I^-/I_3^- electrolyte was prepared in 5 mL batches with the following mixture. Firstly, the solid materials were measured in the following amounts for a 5 mL sample: 0.0300 g Guanidine thiocyanate, 0.0500 g Iodine, 0.0165 g Lithium Iodine, 0.7950 g 1-Butyl-3-methylinidazolim, and 0.1980 g Tert-butyl-pyridine. These materials were added to a small glass vial, and the glass vial was covered with aluminum foil. Valenonitrile and Acetonitrile were added to the covered glass vial in a 0.15:0.85 ratio, respectively, and the vial was shaken by hand to mix the solution. The solution was sealed and stored in a dark and dry environment when not in use.

The counter electrode was prepared by dispersion 0.2000 g of the commercial carbon material in 2 mL of 2-propanol, and hand grinding in a mortar and pestle for 10 minutes. For the AC, MC, and graphite dispersions, a single drop of PTFE was added as a binding material, which was not used for the graphene solutions, due to PTFE increasing aggregation of the graphene particles. The carbon-based dispersion with PTFE was then ground for another 5 minutes, with 2-

propanol added as necessary to maintain the solution viscosity. The mixture was drop cast onto an area of approximately 1.5 cm^2 on a conductive graphite paper electrode, cut into 3-cm by 1-cm strips. The electrodes were allowed to air dry.

To complete the solar cell module, the TiO_2/N3 photoanode was removed from the dye solution, and the excess dye was cleaned from the surface. The active TiO_2/N3 area was isolated by tape placed on the rest of the conductive FTO surface, and 4-5 drops of I^-/I_3^- electrolyte were dropped onto the photoanode to ensure full coverage and contact. The carbon-based counter electrode was used to sandwich the structure and backed by a non-conductive glass slide. The full structure was clamped together to establish full contact between the layers and reduce the amount of electrolyte leakage. This completed DSSC was then used for characterization.

3.3: Fabrication of Carbon-Based Supercapacitor

The carbon-based electrodes were prepared as described in section 3.2: 0.2000 g of the carbon material was dispersed in 2 mL of 2-propanol, and hand ground in a mortar and pestle to make the particle size uniform and well-dispersed. After 10 minutes, a drop of PTFE solution was added to the AC, MC, and graphite solutions and ground for another 5 minutes. The graphene solution was ground for 15 minutes without additives to reduce the aggregation of the particles. The ground solutions were drop cast onto graphite paper sheets cut into 3-cm by 1-cm strips, resulting in a coated area of 1.5 cm^2. The coated electrodes, two for each supercapacitor device, were allowed to air dry overnight. The mass of the strips, before and after the modifying material were added was recorded.

A PVA-KOH hydrogel polymer was fabricated to act as the supercapacitor electrolyte [13, 111]. To prepare the hydrogel, 0.05 g mL^{-1} PVA was added in stages to distilled water and

magnetically stirred at 300 RPM while under cover and heating to 106°C. The solution was stirred until the PVA was dissolved, appearing as a homogenous, moderately opaque, liquid. After dissolution of the PVA, 3 M KOH was added to the solution and mixed until homogenous. Once fully homogenous, Glycerin was added to the mixture in a 1:20 volume ratio and stirred until a fully combined and moderately viscous solution was obtained. The viscous solution was removed from heat and poured into a small petri-dish to air-dry overnight. The resulting hydrogel was white in color and approximately 0.5-1 mm in thickness, capable of acting as both the electrolyte and separator in the EDLC module.

The EDLC module fabrication was completed by sandwiching the PVA-KOH gel electrolyte between two carbon-based electrode that were back by non-conductive glass. The sheets with glass backing were clamped together to guarantee full contact between the layers. This completed supercapacitor was then used for characterization.

3.4: Integrated Cell Assembly

The DSSC photoanode, and electrolytes for both the DSSC and EDLC were fabricated as described in sections 3.2 and 3.3, connected directly by an intermediate, double-sided electrode. The intermediate electrode was fabricated by drop casting the as-prepared carbon-based material in sections 3.2 and 3.3, then flipping the graphite paper and coating an equal area on the opposite side, creating a double-sided electrode. The DSSC module of the device with the applied electrolyte was attached to one side of the intermediate electrode, acting as the CE for the DSSC. The other side of the intermediate electrode acted as the other EDLC electrode with the PVA-KOH hydrogel electrolyte. The full structure is illustrated in Figure 13. The EDLC side of the integrated

device was capped with a slide of non-conductive glass and clamped together to establish good contact between layers. The completed device was then used for characterization.

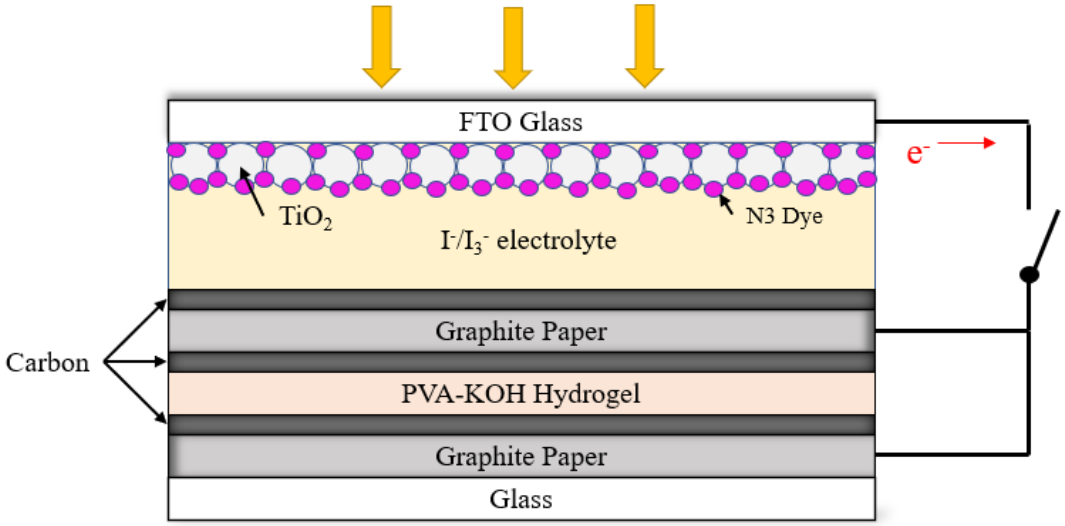

Figure 13: Device structure for the integrated, three-electrode, photo-supercapacitor. The structure consists of a DSSC and carbon-based EDLC, both sharing a common intermediate electrode.

3.5: Characterization Methods

Several characterization techniques were utilized to characterize the commercial material's structure and determine the performance of the integrated device. All techniques for ascertaining the device performance were performed on a Biologic SP-50e Potentiostat, using programs made on the EC-lab software.

The commercial carbon materials were characterized by X-Ray Diffraction analysis (Rigaku Miniflex) between 10° and 70°, step size 0.01, used to determine the crystallinity, and particle size of the carbon substances. The morphology of the structures were determined by Scanning Electron Microscopy (Thermoscientific Phenom Pharos).

The current-voltage (IV) test was used on the solar cell prior to and after integration with the supercapacitor module. During this test, the solar cell was exposed to simulated light at a known intensity to evaluate the performance of the cell components. The performance is evaluated through the short circuit current (I_{sc}), open circuit voltage (V_{oc}), fill factor (FF) and the solar conversion efficiency (η_{sc}). The test was performed under 100 mW cm^{-2} of illumination, cast by a Xenon lamp in standard atmospheric conditions. For this test, the working lead was connected to the graphite paper of the CE, and the counter reference lead was connected to the conductive FTO slide as the photoanode. From the IV curves collected during the test, the fill factor is calculated from the maximum power reached during the test, P_{max} (mW), the V_{oc} (V), and the J_{sc} (mA), in equation 1. These values are used along with the solar intensity, E (mW cm^{-2}), and the photoanode surface area, A_c (cm^{-2}), to determine the solar conversion efficiency in equation 2.

$$FF = \frac{P_{max}}{V_{oc} \cdot J_{sc}} \tag{1}$$

$$\eta_{sc} = \frac{P_{max}}{E \cdot A_c} \tag{2}$$

Constant Current (IT) and Constant Voltage (VT) tests were used to determine the performance of the integrated device, by measuring the amount of voltage and current being transferred to the supercapacitor module from photocharging. Both tests were performed under identical conditions to the IV test, in a two-electrode format. For the IT test, the working lead was connected to the photoelectrode, and the counter reference lead was connected to the external supercapacitor electrode. The leads were switched in the VT test to maintain a positive measurement for fewer post-processing operations. During these tests, a baseline current and

voltage were determined, then the cells were photocharged under 100 mW cm^{-2} illumination and discharged in the dark to measure the discharge time.

Cyclic voltammetry (CV) was used to analyze the electrocatalytic activity of the EDLC module and the device following integration. This test involved cycling the cell between 0 and 1 V working potentials at different scan rates of 2, 5, 10, 50, and 100 mV s^{-1}, measuring how current in the supercapacitor changed during the cycle over a total of 3 cycles. For the integrated device, the working lead was connected to the intermediate electrode, and the counter reference lead was connected to the external supercapacitor electrode. This test was used to calculate the specific capacitance, C_s in F g^{-1}, since the mass of the electrode material was known. From the CV curve collected during the test, the C_s was calculated from the cathodic area, $\int I \cdot dV$ (mA-V), the active mass of the electrodes, m (g), the scan rate, v (mV s^{-1}), and the working potential window, ΔV (V). The equation for C_s is outlined in equation 3 [30, 111].

$$C_s = \frac{\int I \cdot dV}{m \cdot v \cdot \Delta V} \tag{3}$$

Galvanostatic Charge-Discharge (GCD) served to analyze the performance of the non-integrated EDLC module in a two-electrode format. The potential window for the cell operated between 0 and 1 V, and the test measured a driving current of 1-5 mA, for a total of 5 tests with 10 cycles each. The C_s for this test type was calculated with equation 4, utilizing the collected applied current, I (A), the discharge time in seconds, Δt, and the voltage potential window. The C_s from these plots was used to determine the energy (E_{cell}) and power (P_{cell}) density of the cells in equations 5 and 6, with the units W-h kg^{-1} and W kg^{-1} respectively [30, 111].

$$C_s = \frac{I \cdot \Delta t}{\Delta V \cdot m} \quad (4)$$

$$E_{cell} = \frac{1}{2} C \cdot \Delta V^2 \cdot \frac{1000}{3600} \quad (5)$$

$$P_{cell} = \frac{E_{cell}}{\Delta t} \cdot 1000 \quad (6)$$

CHAPTER 4

RESULTS AND DISCUSSION

4.1: Material Characterization

The scanning electron microscope (SEM) imaging of each carbon-material are shown in Figure 14. It is analyzed from this figure that the four carbon-materials have a large difference in surface morphology and particle size. Both AC (Fig. 14A) and MC (Fig. 14B) appear as particulates of varying size with porous structures, although MC appears as a more consistent size and shape having an average particle size of 2.0 μm with a large number of pores on the surface of each particulate. The AC particles have a larger average size at 8.3 μm. The feather-like sheets and layered structure of graphene (Fig. 14C) and graphite (Fig. 14D), respectively, are also seen in high detail. The graphene layer size was approximated to be 33 μm. The large graphite structures with a layer size of approximately 313 μm appear more plate-like than the other structures with few large pores able to increase the active surface area. A large active surface area would absorb more of the electrolyte which is important for the performance of gel-based electrolytes [13]. From these surface morphologies and particle sizes, AC, MC, and graphene are expected to have higher capacitive performance than the graphite-based cells due in part to the particle and pore size.

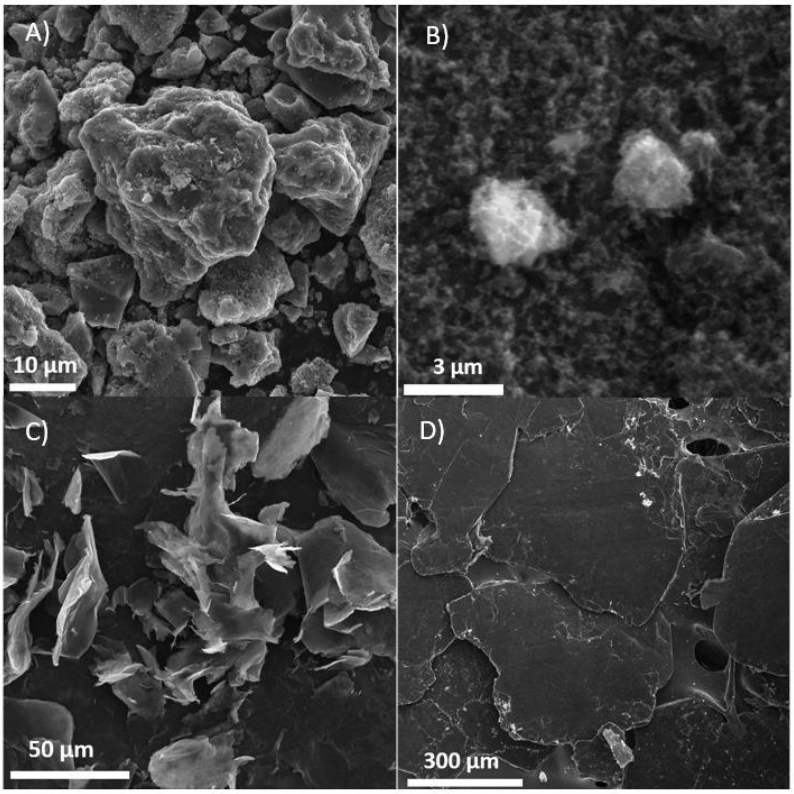

Figure 14: SEM images of A) Activated Carbon, B) MC, C) Graphene, and D) Graphite

The material and crystalline morphology were confirmed through XRD, shown in Figure 15. Both AC and MC show amorphous properties indicative of non-uniform particles in the mixture. The AC peaks occur at 2θ = 22.3° and 44.2° representing a lattice size d_{hkl} = 3.98 Å, and a crystalline size D = 8.23 nm. Similarly, the MC peaks occur at 2θ = 24.6° and 44.0° representing d_{hkl} = 3.62 Å, and D = 15.1 nm. Unlike AC and MC, Graphene and Graphite show highly crystalline peaks occurring at 2θ = 26.5°, and 2θ = 26.4°, respectively. The lattice size and crystalline size for graphene were d_{hkl} = 3.36 Å and D = 130 nm, and for graphite d_{hkl} = 3.37 Å and D = 167 nm.

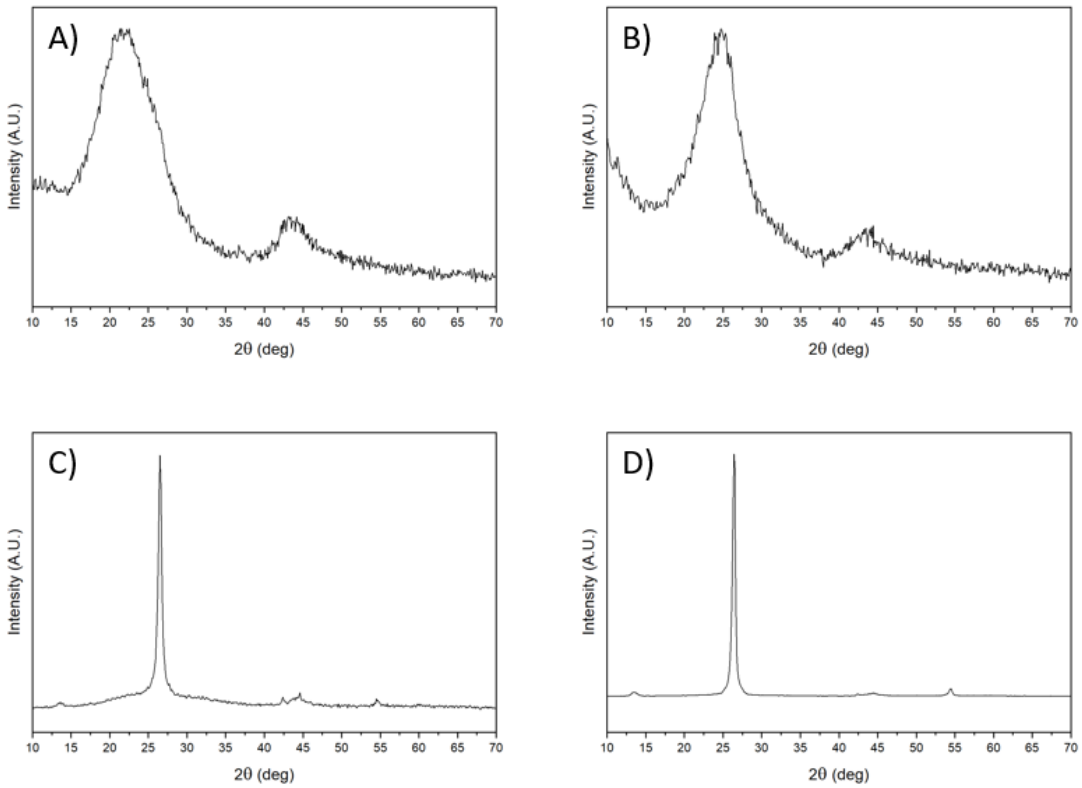

Figure 15: XRD plots for A) Activated Carbon, B) Mesoporous Carbon, C) Graphene, and D) Graphite

4.2: DSSC Performance

The I-V curves of the different carbon-based counter electrode materials are shown in Figure 16, these results as compared before and after integration with the supercapacitor module are also tabulated in Table 3. Prior to integration, the DSSC utilizing a graphite CE showed the greatest efficiency, η_{sc} = 3.26%, with a current density of (J_{sc}) of 7.44 mA cm^{-1}, an open circuit voltage (V_{oc}) of 0.763 V, and a fill factor (FF) of 0.5752. Following integration, the MC CE cells showed J_{sc} = 6.52 mA cm^{-1}, V_{oc} = 0.762 V, FF = 0.625, and a conversion efficiency of 3.10%. This change in maximum power conversion efficiency (PCE) before and after integration for the graphite, AC, and graphene cells was attributed to the decrease in current density over time as the

cell aged and became less stable, and the effects of charging the supercapacitor module. This decrease can be seen directly in Figure 16B as a lowered current density and fill factor. The MC CE cells break this trend, showing improved performance following integration despite lowered short circuit current, attributed to the increase in fill factor observed. The potential reasoning for the poor graphene performance as a CE despite the favorable active surface area and known favorable qualities could be due to the poor uniformity of the flake size, and difficulty in layering the material using the drop cast method.

TABLE 5

DSSC PHOTOVOLTAIC CHARACTERISTICS

	Pre-Integration				Post-Integration			
Cell	J_{sc} (mA cm^{-2})	V_{oc} (V)	FF	η_{sc}	J_{sc} (mA cm^{-2})	V_{oc} (V)	FF	η_{sc}
Graphite	7.44	0.763	0.575	3.26	5.72	0.763	0.489	1.43
AC	6.80	0.713	0.592	2.86	6.44	0.720	0.524	2.43
MC	6.76	0.762	0.591	3.04	6.52	0.762	0.625	3.10
Graphene	6.44	0.738	0.598	2.85	6.32	0.678	0.520	2.22

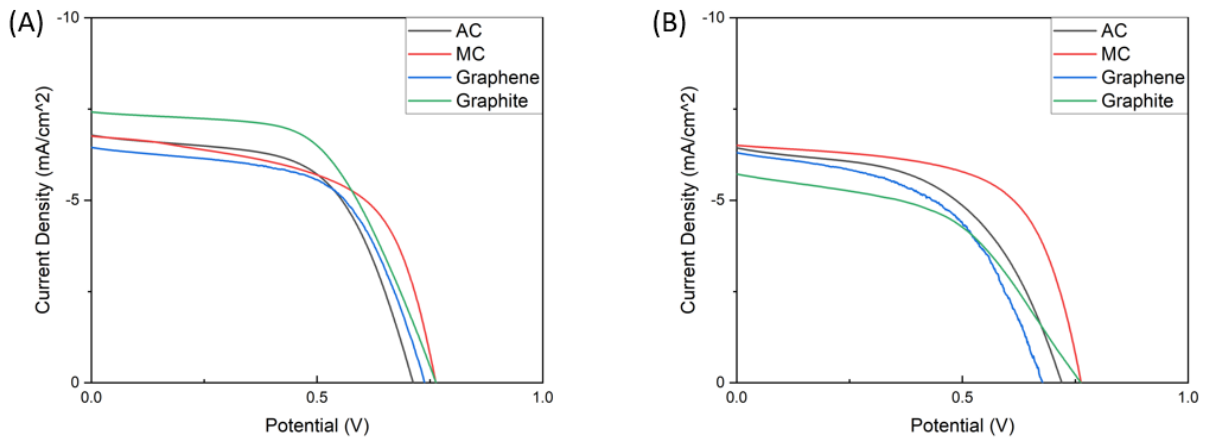

Figure 16: Measured IV curves for the DSSC. (A) IV curves pre-integration with the EDLC. (B) IV curves post-integration with the EDLC.

4.3: Supercapacitor Performance

The energy storage properties of the carbon and PVA-KOH hydrogel supercapacitor prior to integration were analyzed using CV and GCD tests in a two-electrode system. These cells were expected to utilize electric double layer capacitance, with no electron transfer or redox reaction [14, 31, 137]. This mechanism is confirmed for the four different electrode materials at varying scan rates as illustrated in Figure 17A-D. The four materials show roughly quasi-rectangular voltammograms, with no indicated peaks, implying characteristics of EDLC devices [138-141]. As the scan rate was increased from 2 mV s^{-1} to 100 mV s^{-1} the peaks and capacitive area increased. The maximum mass specific capacitance calculated from the cathodic area of the voltammograms at a 2-mV s^{-1} scan rate were 22.0 F g^{-1}, 43.7 F g^{-1}, 21.0 F g^{-1}, and 22.7 F g^{-1}, for the AC, MC, Graphene, and Graphite electrodes, respectively. These values at a scan rate of 2 mV s^{-1} are reported with the energy density and power density from the GCD test in Table 4.

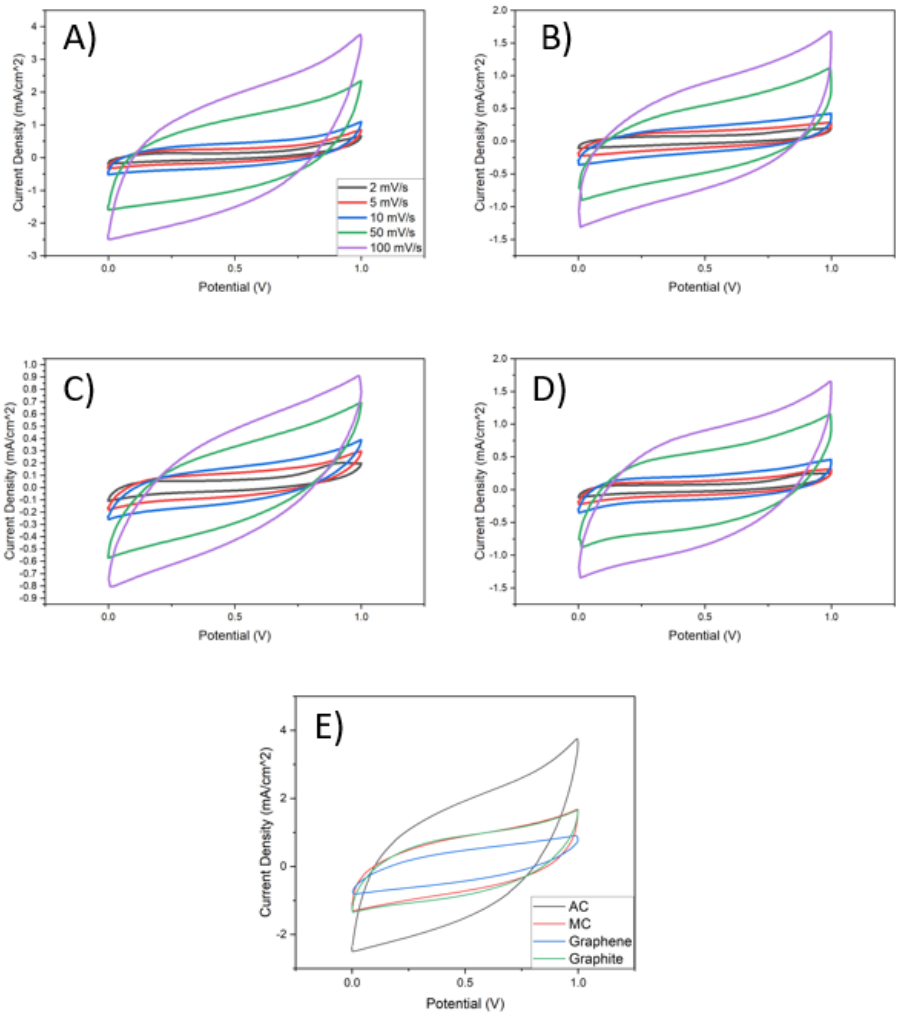

Figure 17: Cyclic Voltammograms for EDLC device using commercial A) Activated Carbon, B) Mesoporous Carbon, C) Graphene, D) Graphite, and E) comparison of 100 mV s^{-1} scan rate.

The relative area of the CV curves for the four materials are compared in Figure 17E at a scan rate of 100 mV s^{-1}. The AC supercapacitor operated with the highest voltammogram area but does not achieve the highest mass specific capacitance compared to MC. This was mainly attributed to the effect of particle surface area, pore size, and density, which are expected to have a large effect on the mass specific capacitance [142-145]. The surface area and pore size were

measured using nitrogen absorption, revealing that MC had the largest pore size, allowing for more penetration of the gel-electrolyte as compared to the other materials.

TABLE 6

EDLC ELECTROCHEMICAL CHARACTERISITICS

Material	Graphite	AC	MC	Graphene
BET Surface area (m^2/g)	7	854	10	186
Pore size (nm)	2-3	2-3	100-150	60-100
C_{sp} (CV, F g^{-1})	22.7	22.0	43.7	21.0
Energy Density (Wh kg^{-1})	0.682	1.12	1.67	0.523
Power Density (W kg^{-1})	52.4	29.6	103	59.1
Coulombic Efficiency (%)	53.2	48.7	67.5	43.7

Note: CV scan rate at 2 mV s^{-1}. GCD scan rate at 1 mA.

The GCD test was used to further analyze the energy storage properties and stability of the carbon-based supercapacitor. Scan rates between 1 mA – 5 mA were used and are displayed in Figure 18. All four curves are roughly triangular, further confirming the EDLC mechanism [31, 85, 146]. The mass specific capacitance calculated from these curves decreased as the charge/discharge rate was increased, resulting in the highest energy and power density at the 1 mA charge/discharge rate. In contrast the coulombic efficiency of the materials increased as the constant current scan rate was increased. The measured coulombic efficiency of the devices,

reported in Table 4 at 1 mA constant current, implied relatively low stability of the devices, and is reflected in the short discharge times. The fast discharge and low stability were attributed to the incompatibility of the PVA-KOH with the electrode materials, and the unreliability of drop cast fabrication for uniform electrodes, specifically for the graphene electrodes, which performed under expectations based on particle surface area and pore size [32, 147].

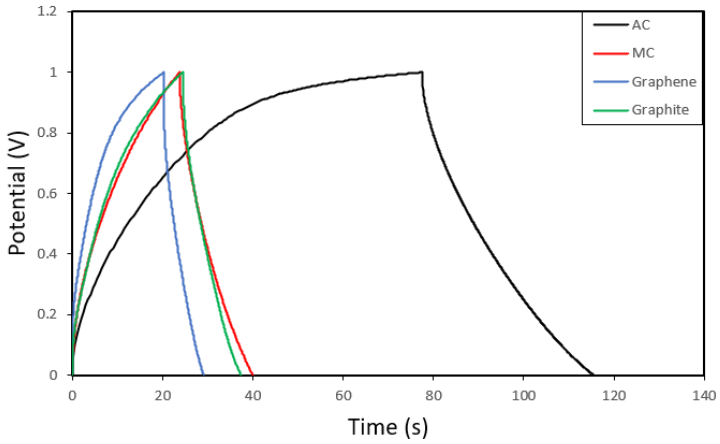

Figure 18: Charge/Discharge curves at 1 mA current scan rate for the four carbon-based electrode materials

The stability of the device after a number of cycles is an important parameter for the functionality of the materials and the longevity of the modules. A supercapacitor was chosen to integrate with the DSSCs due to the high stability of the energy storage device over other types of chemical storage. The stability of the four types of supercapacitor and the integrated device was evaluated using GCD testing over 10 cycles. Over these 10 cycles, the capacitance retention is shown in Figure 19A. Overall, for each capacitor, there is a change in capacitance of less than 2.7%. The AC-based supercapacitor has the least change in capacitance from the initial cell, changing less than 0.2% overall, supported by the consistent shape of the GCD curves in Figure

19B. The MC-based supercapacitor is the least stable of the cells over 10 cycles showing an overall loss in capacitance, remaining within 2.7% of the initial measured specific capacitance, indicated by the slight narrowing of the GCD curves in Figure 19C. The graphene-based supercapacitor has some fluctuation in the measured capacitance over the tested cycles but has an overall loss that is the second highest, and the shortest discharge time as illustrated in Figure 19D. Finally, the graphite-based supercapacitor was the second most stable, showing an overall loss in capacitance of 0.8%, as illustrated in Figures 19A and 19E.

The stability of the device indicated by these 10 cycles is relatively high for the AC, graphene, and graphite supercapacitors. Despite operating with the highest specific capacitance, the MC EDLC has the lowest capacitance retention. Although 10 cycles are a short period as compared to the overall expected life cycle of this type of supercapacitor, this number of cycles can still provide valuable insight into how the stability of the cell can fluctuate over a short term, eventually compounding over time.

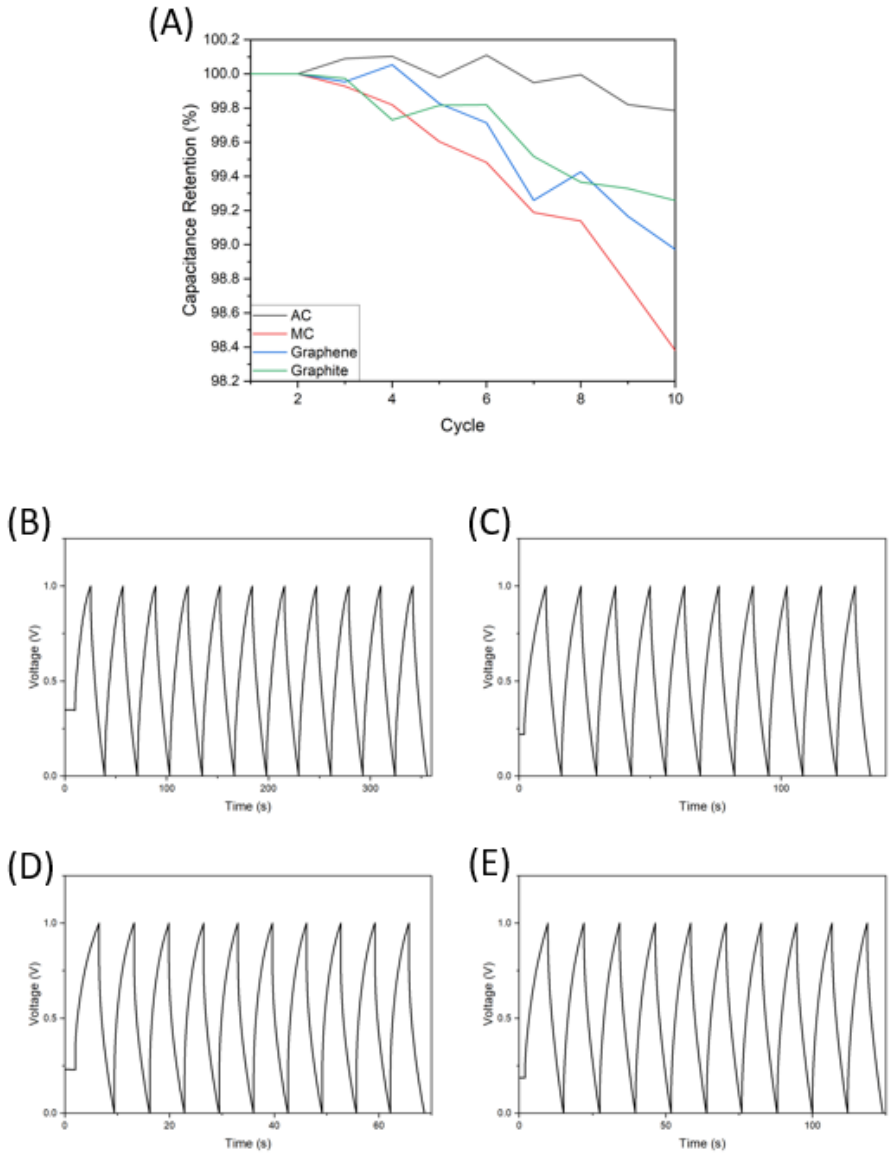

Figure 19: Stability of supercapacitor from GCD measurements. (A) Capacitance retention over 10 cycles for the four types of supercapacitor materials. (B-E) GCD curves over 10 cycles at 2 mA scan rate. (B) Activated Carbon, (C) Mesoporous Carbon, (D) Graphene, and (E) Graphite.

4.4: Integrated Device Performance

Following integration with the supercapacitor module, IT and VT tests were performed to confirm the DSSC was charging the supercapacitor. As indicated in Figure 20A, when the device

was photo-charged, it saw an immediate photocurrent up to 1.63 mA, 1.37 mA, 1.42 mA, and 1.35 mA for AC, MC, graphene, and graphite, respectively. This current decayed during the process as the supercapacitor was charged, consistent with other reported data [34, 105, 107, 108, 111]. The reason for this decay relates to the injection of generated charge into the EDLC module, decaying as the device neared a full charge. Finally, when the light was removed, the current returned to zero, showing that the charging stopped. A small negative current was observed within the few seconds of the light being removed; this negative current could likely represent a slight discharge in the supercapacitor, used to recombine the DSSC redox electrolyte as it self-discharged. The charging voltage for the device was determined from the VT curve. When the device was photo-charged, a charging voltage was observed. As observed in Figure 20B, this charging voltage was greatest for the MC device at 0.536 V, and lowest for the Graphene device at 0.387 V. The device was then allowed to self-discharge to evaluate the storage ability. From the low conversion efficiency, charging voltage, and current, the graphene cells were observed to have very low conversion and storage capability despite the large surface area and ability of graphene-modified devices in literature [111, 145, 148, 149]. The low performance in this report was attributed to the preparation of the cells on the conductive substrate and the small surface area and pore size of the commercially available materials. For the other devices, the fast self-discharge and highly negative voltage supports the implication that the charge from the supercapacitor was partially used to regenerate the DSSC module.

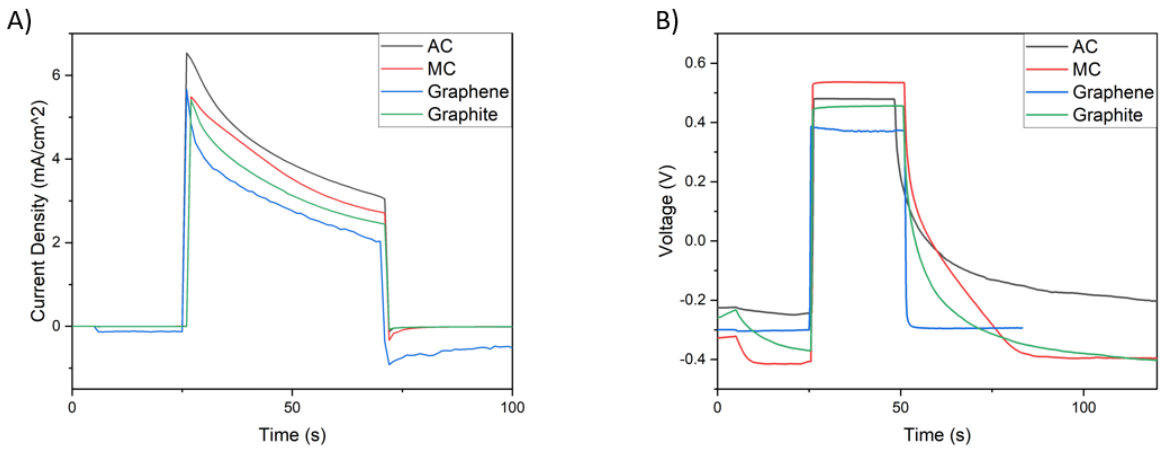

Figure 20: IT and VT curves for the integrated device. A) Current-Time curve for the integrated device during photocharging. B) Voltage-Time curve for the integrated device during photocharging.

Cyclic Voltammetry was also performed following integration to see how the energy storage and stability of the device would be altered under the same conditions. Illustrated in Figure 21A and 21B, the AC and MC devices maintained relatively good ELDC from the roughly rectangular shape of the curves. In the same Figure 21C and 21D, the Graphene and Graphite cells saw a significant breakdown in the EDLC mechanism, showing sharp peaks and large slopes. The same trend as seen in the non-integrated device was noted as the scan rate increased. The mass specific capacitance was calculated from these CV curves, showing a maximum at the 5-mV s^{-1} scan rate. These values were 15.1 F g^{-1}, 40.0 F g^{-1}, 13.0 F g^{-1}, and 15.2 F g^{-1} for the AC, MC, Graphene, and Graphite-based devices, respectively. These values are decreased from the non-integrated devices due to the difference in charging mechanism, and connection to the DSSC module.

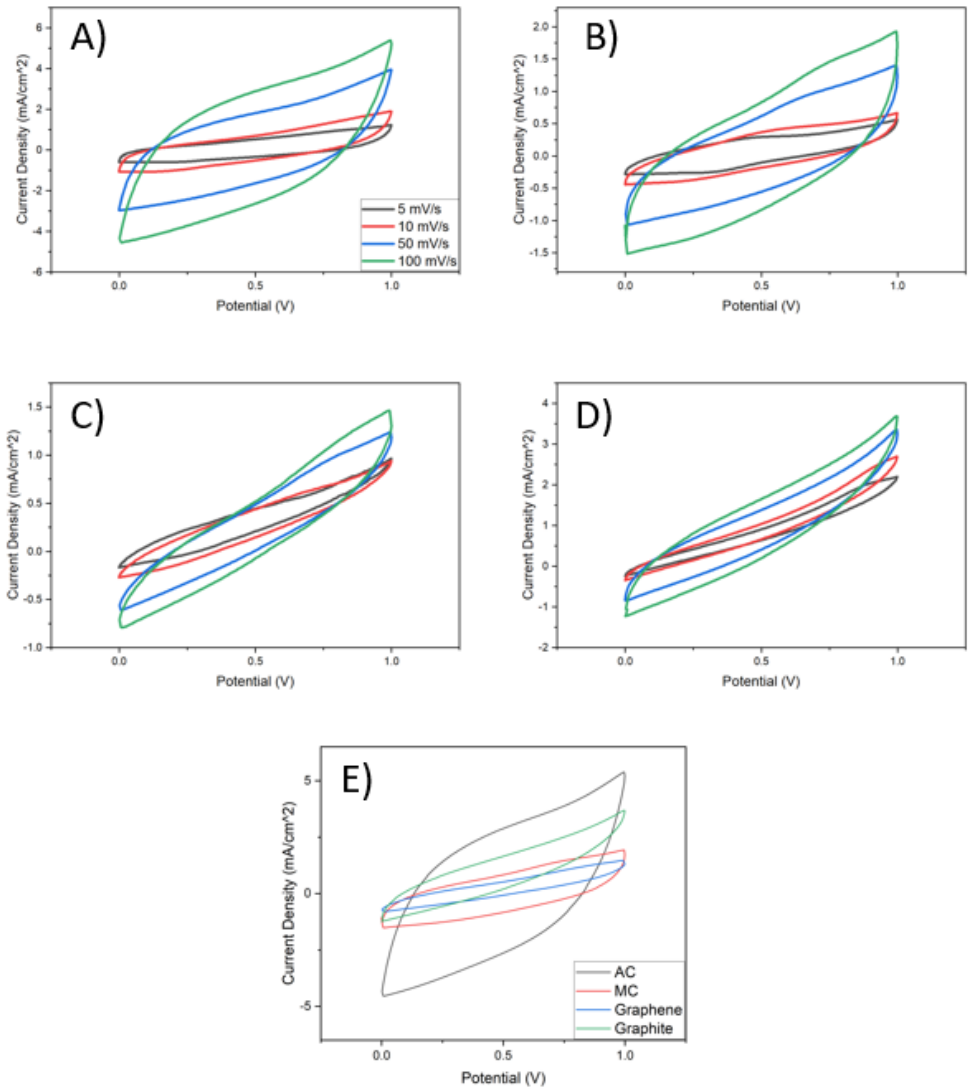

Figure 21: Cyclic Voltammograms for the integrated devices using commercial A) Activated Carbon, B) Mesoporous Carbon, C) Graphene, D) Graphite, and E) for comparison at a 100 mV s^{-1} scan rate.

CHAPTER 5

CONCLUSION

This thesis explored four commercial carbon-based materials for usage in an integrated dye-sensitized solar cell/supercapacitor (DSSCSC) device. For each material, Activated Carbon, Mesoporous Carbon, Graphite, and Graphene, an integrated device was fabricated and tested to determine the utility of the materials based on the device performance. The ultimate goal was to determine if commercial carbon-based materials were compatible with the chosen structure of the device, characterized by the performance of the device. These devices are expected to be ideal for small electronics where large batteries or frequent conventional charging are impractical such as medical devices and sensors.

The fabricated devices were considered three electrode monolithic structures, containing an intermediate electrode made from conductive graphite paper, coated with the active material. The photoelectrode for the device was manufactured from TiO_2 as the semiconductor material, coated on a transparent Fluorine-doped Tin oxide slide, and sensitized by an N3 dye. The counter electrode consisted of the commercial carbon material coated on the double-sided intermediate electrode, with the other side acting as an electrode for the electric double-layer capacitor. The electric double-layer capacitor module had symmetric electrodes made from the commercial carbon materials coated on conductive graphite paper, sandwiching a PVA/KOH aqueous gel electrolyte. The four commercial materials were each used to fabricate the device and achieved different performances.

The DSSC device manufactured with activated carbon performed with the lowest open circuit voltage at 0.713 V and a 2.86% power conversion efficiency pre-integration. Following

integration, the DSSC module saw a slight increase in open circuit voltage to 0.720 V and a photocurrent of 1.63 mA, but a decrease in PCE to 2.43%. The supercapacitor module for this device had a specific capacitance of 22.0 F g^{-1} pre-integration, which decreased to 15.1 F g^{-1} post-integration.

The mesoporous carbon device pre-integration operated with a higher open circuit voltage than the AC electrodes at 0.762 V and had a PCE of 3.04%. Post-integration, the MC-based device was unique, as the fill factor and power conversion efficiency for the device both increased to 0.625 and 3.10% respectively, and a photocurrent of 1.37 mA. The supercapacitor module achieved the best performance out of the trialed materials, being 43.7 F g^{-1} pre-integration, and 40.0 F g^{-1} post-integration. Despite the consistent performance before and after integration, this supercapacitor was also determined to be the least stable as it aged, showing the least capacitance retention over the tested cycles.

The graphite-based device had interestingly mixed results pre- and post-integration. Pre-integration, the DSSC module achieved the highest power conversion efficiency of the four materials at 3.26%, along with the highest open circuit voltage (0.763 V) and closed-circuit current density (7.44 mA cm^{-2}). The supercapacitor module for the material also performed well, having the second highest pre-integration specific capacitance at 22.0 F g^{-1} and 15.2 F g^{-1} post-integration. However, the integrated DSSC module performed the worst out of the four materials, with a power conversion efficiency of only 1.43%.

Similar to the graphite devices, the graphene-based cells had mixed results, that were much lower than expected than the material characterization would suggest. The DSSC pre-integration operated with the lowest power conversion efficiency at only 2.85%. The specific capacitance for the device pre-integration was also the lowest at 21.0 F g^{-1}. The performance decreased further,

although not to the same degree as the graphite cells, following integration. The integrated power conversion efficiency was 2.22%, and the specific capacitance was the lowest at 13.0 F g^{-1}. The reason for the low results was attributed to the simplistic fabrication methods.

The results of these experiments presented in this thesis revealed the utility of these materials as electrodes in monolithic dye sensitized solar cells integrated with a supercapacitor into a singular device. Based on these results, these four materials show promise as inexpensive counter electrodes and as electric double-layer electrodes in an integrated device. Of the commercial materials, mesoporous carbon has the highest overall performance, operating above other researched early devices in the literature, and is the most compatible with the monolithic structure. The alternative commercial materials also have promising performance that is comparable to other researched devices, but such as graphene, are limited by the fabrication methods used, and will require improvements in these methods in order to become more competitive for ultimate commercialization.

CHAPTER 6

FUTURE WORK

Moving forward with this topic, I would recommend fabricating devices with more effective manufacturing methods and a wider range materials, focusing on increasing capacitive performance and stability. The current materials are inexpensive alternatives and can be used for a number of tests with this structure and alternative solar cell types. A hybrid supercapacitor can also be attempted with this layout and these commercial materials as one electrode, in order to determine the further compatibility of this structure and intermediate electrode with DSSCs.

These commercial materials can also be used to evaluate the monolithic structures using alternative third-generation solar cell types, such as perovskite, which can used carbon-materials as the hole transport material. Beyond alternative solar cell types, different layouts like the shared-substrate structure can also be attempted with these materials to evaluate the performance associated with different manufacturing processes.

REFERENCES

REFERENCES

1. Yury, G. and B. Anasori, *The rise of MXenes.* Acs Nano, 2019. **13**: p. 8491-8494.

2. Elavarasan, R.M., *The Motivation for Renewable Energy and its Comparison with Other Energy Sources: A Review.* European Journal of Sustainable Development Research, 2019. **3**(1).

3. Holdren John, P., *Science and Technology for Sustainable Well-Being.* Science, 2008. **319**(5862): p. 424-434.

4. Barnham, K.W.J., M. Mazzer, and B. Clive, *Resolving the energy crisis: nuclear or photovoltaics?* Nature Materials, 2006. **5**(3): p. 161-164.

5. Birel, Ö., S. Nadeem, and H. Duman, *Porphyrin-based dye-sensitized solar cells (DSSCs): a review.* Journal of fluorescence, 2017. **27**(3): p. 1075-1085.

6. Halkos, G.E. and E.-C. Gkampoura *Reviewing Usage, Potentials, and Limitations of Renewable Energy Sources*. Energies, 2020. **13**, DOI: 10.3390/en13112906.

7. Ould Amrouche, S., et al., *Overview of energy storage in renewable energy systems.* International Journal of Hydrogen Energy, 2016. **41**(45): p. 20914-20927.

8. Fagiolari, L., et al., *Integrated energy conversion and storage devices: Interfacing solar cells, batteries and supercapacitors.* Energy Storage Materials, 2022. **51**: p. 400-434.

9. Koksbang, R. and J. Barker, *Solid-state photovoltaic power and battery unit.* Journal of Power Sources, 1995. **55**(2): p. 259-262.

10. Wang, L., et al., *Photo-rechargeable batteries and supercapacitors: Critical roles of carbon-based functional materials.* Carbon Energy, 2021. **3**(2): p. 225-252.

11. Huang, B., et al., *Recycling of lithium-ion batteries: Recent advances and perspectives.* Journal of Power Sources, 2018. **399**: p. 274-286.

12. Hou, Y., R. Vidu, and P. Stroeve, *Solar Energy Storage Methods.* Industrial & Engineering Chemistry Research, 2011. **50**(15): p. 8954-8964.

13. Ur-Rehman, H., et al., *Investigation of charge and current dynamics in PVA–KOH gel electrolyte-based supercapacitor.* Journal of Materials Science: Materials in Electronics, 2022. **33**(5): p. 2322-2335.

14. Libich, J., et al., *Supercapacitors: Properties and applications.* Journal of Energy Storage, 2018. **17**: p. 224-227.

15. Nordin, N.A., et al., *Integrating Photovoltaic (PV) Solar Cells and Supercapacitors for Sustainable Energy Devices: A Review.* Energies, 2021. **14**(21).

16. Liu, R., et al., *Integrated solar capacitors for energy conversion and storage.* Nano Research, 2017. **10**(5): p. 1545-1559.

17. Inganäs, O. and V. Sundström, *Solar energy for electricity and fuels.* Ambio, 2016. **45**(1): p. 15-23.

18. Kloprogge, J.T. and B.J. Wood, *Handbook of Mineral Spectroscopy: Volume 1: X-ray Photoelectron Spectra*. 2020: Elsevier.

19. Tiantian Zhang, H., *Chapter 7—high efficiency plants and building integrated renewable energy systems.* Handbook of energy efficiency in buildings, 2019: p. 441-595.

20. Moon, M.M.A., et al., *Comparative Study of the Second Generation a-Si:H, CdTe, and CIGS Thin-Film Solar Cells.* Advanced Materials Research, 2019. **1154**: p. 102-111.

21. Yan, J. and B.R. Saunders, *Third-generation solar cells: a review and comparison of polymer: fullerene, hybrid polymer and perovskite solar cells.* Rsc Advances, 2014. **4**(82): p. 43286-43314.

22. Conibeer, G., *Third-generation photovoltaics.* Materials Today, 2007. **10**(11): p. 42-50.

23. Devadiga, D., et al., *Dye-Sensitized Solar Cell for Indoor Applications: A Mini-Review.* Journal of Electronic Materials, 2021. **50**(6): p. 3187-3206.

24. Freitag, M., et al., *Dye-sensitized solar cells for efficient power generation under ambient lighting.* Nature Photonics, 2017. **11**(6): p. 372-378.

25. Scalia, A., et al., *High energy and high voltage integrated photo-electrochemical double layer capacitor.* Sustainable Energy & Fuels, 2018. **2**(5): p. 968-977.

26. Iwata, S., et al., *Stability of the current characteristics of dye-sensitized solar cells in the second quadrant of the current–voltage characteristics.* Energy Reports, 2018. **4**: p. 8-12.

27. Devadiga, D., et al., *Recent progress in dye sensitized solar cell materials and photo-supercapacitors: A review.* Journal of Power Sources, 2021. **493**: p. 229698.

28. Ng, C.H., et al., *Potential active materials for photo-supercapacitor: A review.* Journal of Power Sources, 2015. **296**: p. 169-185.

29. Paul, R., et al., *Characterization techniques and analytical methods of carbon-based materials for energy applications,* in *Carbon based nanomaterials for advanced thermal and electrochemical energy storage and conversion*. 2019, Elsevier. p. 63-88.

30. Kar, K.K., *Handbook of Nanocomposite Supercapacitor Materials I: Characteristics*. Vol. 300. 2020: Springer Nature.

31. Kar, K.K., *Handbook of Nanocomposite Supercapacitor Materials II: Performance*. Vol. 302. 2020: Springer Nature.

32. Pal, B., et al., *Electrolyte selection for supercapacitive devices: a critical review.* Nanoscale Advances, 2019. **1**(10): p. 3807-3835.

33. Raghavendra, K.V.G., et al., *An intuitive review of supercapacitors with recent progress and novel device applications.* Journal of Energy Storage, 2020. **31**: p. 101652.

34. Miyasaka, T. and T.N. Murakami, *The photocapacitor: An efficient self-charging capacitor for direct storage of solar energy.* Applied Physics Letters, 2004. **85**(17): p. 3932-3934.

35. Murakami, T.N., N. Kawashima, and T. Miyasaka, *A high-voltage dye-sensitized photocapacitor of a three-electrode system.* Chemical Communications, 2005(26): p. 3346-3348.

36. Kulesza, P.J., et al., *Development of Solid-State Photo-Supercapacitor by Coupling Dye-Sensitized Solar Cell Utilizing Conducting Polymer Charge Relay with Proton-Conducting Membrane Based Electrochemical Capacitor.* ECS Transactions, 2013. **50**(43): p. 235-244.

37. Fraas, L.M. and L.D. Partain, *Solar cells and their applications*. 2010: John Wiley & Sons.

38. Vasiliev, M., M. Nur-E-Alam, and K. Alameh *Recent Developments in Solar Energy-Harvesting Technologies for Building Integration and Distributed Energy Generation*. Energies, 2019. **12**, DOI: 10.3390/en12061080.

39. Yeoh, M.E. and K.Y. Chan, *A Review on Semitransparent Solar Cells for Real-Life Applications Based on Dye-Sensitized Technology.* IEEE Journal of Photovoltaics, 2021. **11**(2): p. 354-361.

40. Malara, F., et al., *Smart Windows for Building Integration: A New Architecture for Photovoltachromic Devices.* ACS Applied Materials & Interfaces, 2014. **6**(12): p. 9290-9297.

41. Wang, J., et al., *A review of NiO-based electrochromic-energy storage bifunctional material and integrated device.* Journal of Energy Storage, 2022. **47**: p. 103597.

42. Maitra, A., et al., *Chapter 14 - Advanced self-charging power packs: The assimilation of energy harvesting and storage systems*, in *Sustainable Materials and Green Processing for Energy Conversion*, K.Y. Cheong and A. Apblett, Editors. 2022, Elsevier. p. 441-477.

43. Sahoo, S., et al., *Self-charging supercapacitors for smart electronic devices: a concise review on the recent trends and future sustainability.* Journal of Materials Science, 2022. **57**(7): p. 4399-4440.

44. Pallikkara, A. and K. Ramakrishnan, *Efficient charge collection of photoanodes and light absorption of photosensitizers: A review.* International Journal of Energy Research, 2021. **45**(2): p. 1425-1448.

45. Agrawal, A., et al., *Advancements, frontiers and analysis of metal oxide semiconductor, dye, electrolyte and counter electrode of dye sensitized solar cell.* Solar Energy, 2022. **233**: p. 378-407.

46. Kumar, Y., et al., *Photoanode modified with nanostructures for efficiency enhancement in DSSC: a review.* Carbon Letters, 2023. **33**(1): p. 35-58.

47. Richhariya, G., et al., *Natural dyes for dye sensitized solar cell: A review.* Renewable and Sustainable Energy Reviews, 2017. **69**: p. 705-718.

48. Castillo-Robles, J.A., et al. *Advances on Dye-Sensitized Solar Cells (DSSCs) Nanostructures and Natural Colorants: A Review*. Journal of Composites Science, 2021. **5**, DOI: 10.3390/jcs5110288.

49. Gong, J., et al., *Review on dye-sensitized solar cells (DSSCs): Advanced techniques and research trends.* Renewable and Sustainable Energy Reviews, 2017. **68**: p. 234-246.

50. Ren, Y., et al., *Hydroxamic acid pre-adsorption raises the efficiency of cosensitized solar cells.* Nature, 2023. **613**(7942): p. 60-65.

51. Tomar, N., et al., *Ruthenium complexes based dye sensitized solar cells: Fundamentals and research trends.* Solar Energy, 2020. **207**: p. 59-76.

52. Dhonde, M., et al., *Review—Recent Advancements in Dye-Sensitized Solar Cells; From Photoelectrode to Counter Electrode.* Journal of The Electrochemical Society, 2022. **169**(6): p. 066507.

53. Wang, N., et al., *Current Progress in Solid-State Electrolytes for Dye-Sensitized Solar Cells: A Mini-Review.* Journal of Electronic Materials, 2020. **49**(12): p. 7085-7097.

54. Mahmood, A., *Recent research progress on quasi-solid-state electrolytes for dye-sensitized solar cells.* Journal of Energy Chemistry, 2015. **24**(6): p. 686-692.

55. Wang, X., et al., *Review on Low-Cost Counter Electrode Materials for Dye-Sensitized Solar Cells: Effective Strategy to Improve Photovoltaic Performance.* Advanced Materials Interfaces, 2022. **9**(2): p. 2101229.

56. Karthick, S.N., et al., *Dye-Sensitized Solar Cells: History, Components, Configuration, and Working Principle*, in *Interfacial Engineering in Functional Materials for Dye-Sensitized Solar Cells*. 2019. p. 1-16.

57. Thavasi, V., et al., *Controlled electron injection and transport at materials interfaces in dye sensitized solar cells.* Materials Science and Engineering: R: Reports, 2009. **63**(3): p. 81-99.

58. Greijer Agrell, H., J. Lindgren, and A. Hagfeldt, *Degradation mechanisms in a dye-sensitized solar cell studied by UV–VIS and IR spectroscopy.* Solar Energy, 2003. **75**(2): p. 169-180.

59. Zhang, Y., L. Ye, and J. Hou, *Precise Characterization of Performance Metrics of Organic Solar Cells.* Small Methods, 2017. **1**(8): p. 1700159.

60. Qi, B. and J. Wang, *Fill factor in organic solar cells.* Physical Chemistry Chemical Physics, 2013. **15**(23): p. 8972-8982.

61. Kurzweil, P., *CAPACITORS | Electrostatic Solid-State Capacitors*, in *Encyclopedia of Electrochemical Power Sources*, J. Garche, Editor. 2009, Elsevier: Amsterdam. p. 600-606.

62. Goikolea, E. and R. Mysyk, *Chapter Four - Nanotechnology in Electrochemical Capacitors*, in *Emerging Nanotechnologies in Rechargeable Energy Storage Systems*, L.M. Rodriguez-Martinez and N. Omar, Editors. 2017, Elsevier: Boston. p. 131-169.

63. Li, H., et al., *Quantifying the Volumetric Performance Metrics of Supercapacitors.* Advanced Energy Materials, 2019. **9**(21): p. 1900079.

64. Ge, Y., et al., *How to measure and report the capacity of electrochemical double layers, supercapacitors, and their electrode materials.* Journal of Solid State Electrochemistry, 2020. **24**(11): p. 3215-3230.

65. Sarno, M., *Chapter 22 - Nanotechnology in energy storage: the supercapacitors*, in *Studies in Surface Science and Catalysis*, A. Basile, et al., Editors. 2020, Elsevier. p. 431-458.

66. Muzaffar, A., et al., *A review on recent advances in hybrid supercapacitors: Design, fabrication and applications.* Renewable and Sustainable Energy Reviews, 2019. **101**: p. 123-145.

67. Farsak, M. and G. Kardaş, *2.12 Electrolytic Materials*, in *Comprehensive Energy Systems*, I. Dincer, Editor. 2018, Elsevier: Oxford. p. 329-367.

68. Raza, W., et al., *Recent advancements in supercapacitor technology.* Nano Energy, 2018. **52**: p. 441-473.

69. Forse, A.C., et al., *New Perspectives on the Charging Mechanisms of Supercapacitors.* Journal of the American Chemical Society, 2016. **138**(18): p. 5731-5744.

70. Schoetz, T., et al., *Disentangling faradaic, pseudocapacitive, and capacitive charge storage: A tutorial for the characterization of batteries, supercapacitors, and hybrid systems.* Electrochimica Acta, 2022. **412**: p. 140072.

71. Afif, A., et al., *Advanced materials and technologies for hybrid supercapacitors for energy storage – A review.* Journal of Energy Storage, 2019. **25**: p. 100852.

72. Fleischmann, S., et al., *Pseudocapacitance: From Fundamental Understanding to High Power Energy Storage Materials.* Chemical Reviews, 2020. **120**(14): p. 6738-6782.

73. Yi, C.-q., et al., *Recent advances in pseudocapacitor electrode materials: Transition metal oxides and nitrides.* Transactions of Nonferrous Metals Society of China, 2018. **28**(10): p. 1980-2001.

74. Chen, R., et al., *The Development of Pseudocapacitor Electrodes and Devices with High Active Mass Loading.* Advanced Energy Materials, 2020. **10**(20): p. 1903848.

75. Chen, X., R. Paul, and L. Dai, *Carbon-based supercapacitors for efficient energy storage.* National Science Review, 2017. **4**(3): p. 453-489.

76. Berestok, T., et al., *High-Efficiency Monolithic Photosupercapacitors: Smart Integration of a Perovskite Solar Cell with a Mesoporous Carbon Double-Layer Capacitor.* Solar RRL, 2021. **5**(11): p. 2100662.

77. Kim, J., et al., *A highly efficient self-power pack system integrating supercapacitors and photovoltaics with an area-saving monolithic architecture.* Journal of Materials Chemistry A, 2017. **5**(5): p. 1906-1912.

78. Fu, Y., et al., *Integrated power fiber for energy conversion and storage.* Energy & Environmental Science, 2013. **6**(3): p. 805-812.

79. Sun, Y. and X. Yan, *Recent Advances in Dual-Functional Devices Integrating Solar Cells and Supercapacitors.* Solar RRL, 2017. **1**(3-4): p. 1700002.

80. Yeow, Q.J., et al., *Converting Solar Cells to Photocapacitors without the Incorporation of Additional Capacitive Components.* ACS Applied Energy Materials, 2022. **5**(6): p. 6746-6753.

81. Yilmaz, M., et al., *Integrated photocapacitors based on dye-sensitized TiO2/FTO as photoanode and MnO2 coated micro-array CNTs as supercapacitor counter electrode with TEABF4 electrolyte.* Journal of Renewable and Sustainable Energy, 2018. **10**(6): p. 063503.

82. Zhang, X., et al., *Dye-Sensitized Solar Cell with Energy Storage Function through PVDF/ZnO Nanocomposite Counter Electrode.* Advanced Materials, 2013. **25**(30): p. 4093-4096.

83. Zhang, X. and H. Jiang, *Scattering-layer-induced energy storage function in polymer-based quasi-solid-state dye-sensitized solar cells.* Applied Physics Letters, 2015. **106**(10): p. 103903.

84. K, N. and C.S. Rout, *Photo-powered integrated supercapacitors: a review on recent developments, challenges and future perspectives.* Journal of Materials Chemistry A, 2021. **9**(13): p. 8248-8278.

85. Scalia, A., et al., *Innovative multipolymer electrolyte membrane designed by oxygen inhibited UV-crosslinking enables solid-state in plane integration of energy conversion and storage devices.* Energy, 2019. **166**: p. 789-795.

86. Khatun, F., et al., *In situ synthesized SrF2/polyvinylidene fluoride nanocomposite film based photo-power cell with imperious performance and stability.* Electrochimica Acta, 2018. **282**: p. 194-204.

87. Khatun, F., et al., *Photo-Rechargeable Organic–Inorganic Dye-Integrated Polymeric Power Cell with Superior Performance and Durability.* Langmuir, 2019. **35**(19): p. 6346-6355.

88. Yang, Z., et al., *An integrated device for both photoelectric conversion and energy storage based on free-standing and aligned carbon nanotube film.* Journal of Materials Chemistry A, 2013. **1**(3): p. 954-958.

89. Li, F., et al., *White Light to Near-IR Chargeable Single Component Photocapacitor Based on Donor-chromophore-Acceptor Dyes.* Chemistry – An Asian Journal, 2023. **18**(12): p. e202300188.

90. Liu, R., et al., *An Efficient Ultra-Flexible Photo-Charging System Integrating Organic Photovoltaics and Supercapacitors.* Advanced Energy Materials, 2020. **10**(20): p. 2000523.

91. Yang, Y., et al., *Self-charging flexible solar capacitors based on integrated perovskite solar cells and quasi-solid-state supercapacitors fabricated at low temperature.* Journal of Power Sources, 2020. **479**: p. 229046.

92. Xu, X., et al., *A Power Pack Based on Organometallic Perovskite Solar Cell and Supercapacitor.* ACS Nano, 2015. **9**(2): p. 1782-1787.

93. Dong, P., et al., *A flexible solar cell/supercapacitor integrated energy device.* Nano Energy, 2017. **42**: p. 181-186.

94. Maddala, G., et al., *Optimal Dye Sensitized Solar Cell and Photocapacitor Performance with Efficient Electrocatalytic SWCNH Assisted Carbon Electrode.* ACS Applied Energy Materials, 2021. **4**(10): p. 11225-11233.

95. Shin, J., et al., *Integrated photo-rechargeable supercapacitors formed via electrode sharing.* Organic Electronics, 2021. **89**: p. 106050.

96. Das, A., et al., *Bifunctional Photo-Supercapacitor with a New Architecture Converts and Stores Solar Energy as Charge.* ACS Applied Materials & Interfaces, 2018. **10**(42): p. 35932-35945.

97. Poojari, V., et al., *Conductivity and Electrochemical Behavior of Plasticized Polymer Electrolyte for Dye-Sensitized Solar Cell Integrated Supercapacitor.* Journal of Electrochemical Energy Conversion and Storage, 2020. **17**(3).

98. Diantoro, M., et al., *Effect of (SnO2:TiO2) nanoparticles on charging performance of integrated dye-sensitized solar cell-supercapacitor.* AIP Conference Proceedings, 2020. **2231**(1): p. 040007.

99. Masrul, M.Z., et al., *The Effect of Light Irradiation on Performance of Photo-Supercapacitor of FTO/TiO2-ZnO-β Carotene-Quercetin/Carbon/Al/PVDF-BaTiO3/Al.* IOP Conference Series: Materials Science and Engineering, 2019. **515**(1): p. 012077.

100. Wang, H., et al., *Design bifunctional nitrogen doped flexible carbon sphere electrode for dye-sensitized solar cell and supercapacitor.* Electrochimica Acta, 2020. **334**: p. 135582.

101. Saaid, F.I., et al., *Flower-like nanosheets FeCo2O4 for application in supercapacitor and dye-sensitized solar cell.* Journal of Materials Science: Materials in Electronics, 2022. **33**(7): p. 3648-3669.

102. Peter, I.J., et al., *MWCNT Aided Cobalt Antimony Sulfide Electrocatalyst for Dye-Sensitized Solar Cells and Supercapacitors: Designing Integrated Photo-Powered Energy System.* Journal of The Electrochemical Society, 2022. **169**(5): p. 056518.

103. Wu, M., et al., *Multifunctional boron-doped carbon fiber electrodes synthesized by electrospinning for supercapacitors, dye-sensitized solar cells, and photocapacitors.* Surfaces and Interfaces, 2022. **31**: p. 101983.

104. Scalia, A., et al., *Portable High Voltage Integrated Harvesting-Storage Device Employing Dye-Sensitized Solar Module and All-Solid-State Electrochemical Double Layer Capacitor.* Frontiers in Chemistry, 2018. **6**.

105. Hsu, C.-Y., et al., *A dye-sensitized photo-supercapacitor based on PProDOT-Et2 thick films.* Journal of Power Sources, 2010. **195**(18): p. 6232-6238.

106. Mini, P.A., S.V. Nair, and K.R.V. Subramanian, *Design and development of an integrated device consisting of an independent solar cell with electrical storage capacity.* Progress in Photovoltaics: Research and Applications, 2013. **21**(5): p. 1153-1157.

107. Skunik-Nuckowska, M., et al., *Integration of solid-state dye-sensitized solar cell with metal oxide charge storage material into photoelectrochemical capacitor.* Journal of Power Sources, 2013. **234**: p. 91-99.

108. Bagheri, N., et al., *Combination of Asymmetric Supercapacitor Utilizing Activated Carbon and Nickel Oxide with Cobalt Polypyridyl-Based Dye-Sensitized Solar Cell.* Electrochimica Acta, 2014. **143**: p. 390-397.

109. Xu, J., et al., *Integrated Photo-supercapacitor Based on Bi-polar TiO2 Nanotube Arrays with Selective One-Side Plasma-Assisted Hydrogenation.* Advanced Functional Materials, 2014. **24**(13): p. 1840-1846.

110. Cohn, A.P., et al., *All Silicon Electrode Photocapacitor for Integrated Energy Storage and Conversion.* Nano Letters, 2015. **15**(4): p. 2727-2731.

111. Lau, S.C., et al., *A three-electrode integrated photo-supercapacitor utilizing graphene-based intermediate bifunctional electrode.* Electrochimica Acta, 2017. **238**: p. 178-184.

112. Devadiga, D., et al., *Novel photosensitizer for dye-sensitized solar cell based on ionic liquid–doped blend polymer electrolyte.* Journal of Solid State Electrochemistry, 2021. **25**(4): p. 1461-1478.

113. Das, A., et al., *Redox active and electrically conducting cobalt telluride Nanorods/Poly(1-aminoanthraquinone) composite and photoactive Rose Bengal dye based photo-supercapacitor.* Applied Materials Today, 2020. **19**: p. 100592.

114. Bae, J., et al., *Single-Fiber-Based Hybridization of Energy Converters and Storage Units Using Graphene as Electrodes.* Advanced Materials, 2011. **23**(30): p. 3446-3449.

115. J. Varma, S., et al., *Fiber-Type Solar Cells, Nanogenerators, Batteries, and Supercapacitors for Wearable Applications.* Advanced Science, 2018. **5**(9): p. 1800340.

116. Liao, M., et al., *The Recent Advance in Fiber-Shaped Energy Storage Devices.* Advanced Electronic Materials, 2019. **5**(1): p. 1800456.

117. Peng, M. and D. Zou, *Flexible fiber/wire-shaped solar cells in progress: properties, materials, and designs.* Journal of Materials Chemistry A, 2015. **3**(41): p. 20435-20458.

118. Peng, H., *Fiber-shaped energy harvesting and storage devices*. Vol. 38. 2015: Springer.

119. Weng, W., et al., *Smart Electronic Textiles.* Angewandte Chemie International Edition, 2016. **55**(21): p. 6140-6169.

120. Yao, Y., et al., *Selected functionalization of continuous graphene fibers for integrated energy conversion and storage.* Science Bulletin, 2020. **65**(6): p. 486-495.

121. Chen, T., et al., *An Integrated "Energy Wire" for both Photoelectric Conversion and Energy Storage.* Angewandte Chemie International Edition, 2012. **51**(48): p. 11977-11980.

122. Sun, H., et al., *A Twisted Wire-Shaped Dual-Function Energy Device for Photoelectric Conversion and Electrochemical Storage.* Angewandte Chemie International Edition, 2014. **53**(26): p. 6664-6668.

123. Chen, X., et al., *A novel "energy fiber" by coaxially integrating dye-sensitized solar cell and electrochemical capacitor.* Journal of Materials Chemistry A, 2014. **2**(6): p. 1897-1902.

124. Yang, Z., et al., *Self-Powered Energy Fiber: Energy Conversion in the Sheath and Storage in the Core.* Advanced Materials, 2014. **26**(41): p. 7038-7042.

125. Liang, J., et al., *MoS2-based all-purpose fibrous electrode and self-powering energy fiber for efficient energy harvesting and storage.* Advanced Energy Materials, 2017. **7**(3): p. 1601208.

126. Wang, X., K. Jiang, and G. Shen, *Flexible fiber energy storage and integrated devices: recent progress and perspectives.* Materials Today, 2015. **18**(5): p. 265-272.

127. Liu, K., et al., *A Self-supported Graphene/Carbon Nanotube Hollow Fiber for Integrated Energy Conversion and Storage.* Nano-Micro Letters, 2020. **12**(1): p. 64.

128. He, C., et al., *Bifunctional Shared Fibers for High-Efficiency Self-Powered Fiber-Shaped Photocapacitors.* Advanced Fiber Materials, 2023. **5**(1): p. 130-137.

129. Wang, Z., et al., *Flexible self-powered fiber-shaped photocapacitors with ultralong cyclelife and total energy efficiency of 5.1%.* Energy Storage Materials, 2020. **24**: p. 255-264.

130. Westover, A.S., et al., *Direct integration of a supercapacitor into the backside of a silicon photovoltaic device.* Applied Physics Letters, 2014. **104**(21): p. 213905.

131. Ouyang, Z., et al., *Monolithic Integration of Anodic Molybdenum Oxide Pseudocapacitive Electrodes on Screen-Printed Silicon Solar Cells for Hybrid Energy Harvesting-Storage Systems.* Advanced Energy Materials, 2017. **7**(9): p. 1602325.

132. Meng, H., S. Pang, and G. Cui, *Photo-Supercapacitors Based on Third-Generation Solar Cells.* ChemSusChem, 2019. **12**(15): p. 3431-3447.

133. Takshi, A., et al., *A Critical Review on the Voltage Requirement in Hybrid Cells with Solar Energy Harvesting and Energy Storage Capability.* Batteries & Supercaps, 2021. **4**(2): p. 252-267.

134. Zhao, J., et al., *Recent advances in wearable self-powered energy systems based on flexible energy storage devices integrated with flexible solar cells.* Journal of Materials Chemistry A, 2021. **9**(35): p. 18887-18905.

135. Chirauri, S.K., A.K. Dehury, and Y.S. Chaudhary, *Photosupercapacitors: A perspective of planar and flexible dual functioning devices.* WIREs Energy and Environment, 2020. **9**(6): p. e377.

136. Yang, Y., et al., *Perovskite solar cells based self-charging power packs: Fundamentals, applications and challenges.* Nano Energy, 2022. **94**: p. 106910.

137. Obreja, V.V.N., *On the performance of supercapacitors with electrodes based on carbon nanotubes and carbon activated material—A review.* Physica E: Low-dimensional Systems and Nanostructures, 2008. **40**(7): p. 2596-2605.

138. Lv, Y., et al., *A comprehensive study on KOH activation of ordered mesoporous carbons and their supercapacitor application.* Journal of Materials Chemistry, 2012. **22**(1): p. 93-99.

139. Lewandowski, A., et al., *Supercapacitor based on activated carbon and polyethylene oxide–KOH–H2O polymer electrolyte.* Electrochimica Acta, 2001. **46**(18): p. 2777-2780.

140. Allagui, A., et al., *Reevaluation of Performance of Electric Double-layer Capacitors from Constant-current Charge/Discharge and Cyclic Voltammetry.* Scientific Reports, 2016. **6**(1): p. 38568.

141. Huang, Y.-F., et al., *Boron cross-linked graphene oxide/polyvinyl alcohol nanocomposite gel electrolyte for flexible solid-state electric double layer capacitor with high performance.* Electrochimica Acta, 2014. **132**: p. 103-111.

142. Azam, M.A., et al., *Recent advances in biomass-derived carbon, mesoporous materials, and transition metal nitrides as new electrode materials for supercapacitor: A short review.* International Journal of Energy Research, 2021. **45**(6): p. 8335-8346.

143. Prabaharan, S.R.S., R. Vimala, and Z. Zainal, *Nanostructured mesoporous carbon as electrodes for supercapacitors.* Journal of Power Sources, 2006. **161**(1): p. 730-736.

144. Li, G.-R. and X.-P. Gao, *Low-Cost Counter-Electrode Materials for Dye-Sensitized and Perovskite Solar Cells.* Advanced Materials, 2020. **32**(3): p. 1806478.

145. Du, X., et al., *Graphene nanosheets as electrode material for electric double-layer capacitors.* Electrochimica Acta, 2010. **55**(16): p. 4812-4819.

146. Muramatsu, D., et al., *Preparation and Characterization of Electric Double-Layer Capacitors Having a 3D Stainless-Steel Fiber Sheet as the Current Collector.* ACS Omega, 2022. **7**(23): p. 19216-19224.

147. Kaliyaraj Selva Kumar, A., et al., *A mini-review: How reliable is the drop casting technique?* Electrochemistry Communications, 2020. **121**: p. 106867.

148. Gao, K., D. Ti, and Z. Zhang, *A photocapacitor with high working voltage and energy density.* Sustainable Energy & Fuels, 2019. **3**(8): p. 1937-1942.

149. Tale, B., K.R. Nemade, and P.V. Tekade, *Graphene based nano-composites for efficient energy conversion and storage in Solar cells and Supercapacitors : A Review.* Polymer-Plastics Technology and Materials, 2021. **60**(7): p. 784-797.

APPENDIX

APPENDIX

COPYRIGHT PERMISSIONS

Licensed Content in order of appearance:

Liscence Number: 5663131178578

AIP PUBLISHING LICENSE
TERMS AND CONDITIONS

Nov 06, 2023

This Agreement between Victoria Bishop ("You") and AIP Publishing ("AIP Publishing") consists of your license details and the terms and conditions provided by AIP Publishing and Copyright Clearance Center.

License Number	5663131178578
License date	Nov 06, 2023
Licensed Content Publisher	AIP Publishing
Licensed Content Publication	Applied Physics Letters
Licensed Content Title	The photocapacitor: An efficient self-charging capacitor for direct storage of solar energy
Licensed Content Author	Miyasaka, Tsutomu; Murakami, Takurou N.
Licensed Content Date	Oct 29, 2004
Licensed Content Volume	85
Licensed Content Issue	17
Type of Use	Thesis/Dissertation
Requestor type	Student
Format	Electronic

APPENDIX (continued.)

License Number: 1413772-2

Order Date	06-Nov-2023	Type of Use	Republish in a thesis/dissertation
Order License ID	1413772-2		
ISSN	1359-7345	Publisher	THE SOCIETY,
		Portion	Image/photo/illustration

LICENSED CONTENT

Publication Title	Chemical communications : Chem comm	Publication Type	Journal
		Start Page	3346
Article Title	A high-voltage dye-sensitized photocapacitor of a three-electrode system.	End Page	3348
		Issue	26
		Volume	0
Author/Editor	ROYAL SOCIETY OF CHEMISTRY (GREAT BRITAIN)	URL	http://www.rsc.org/Publishing/Journals/cc/Article.asp?Type=CurrentIssue
Date	01/01/1996		
Language	English		
Country	United Kingdom of Great Britain and Northern Ireland		
Rightsholder	Royal Society of Chemistry		

REQUEST DETAILS

Portion Type	Image/photo/illustration	Distribution	United States
Number of Images / Photos / Illustrations	1	Translation	Original language of publication
Format (select all that apply)	Electronic	Copies for the Disabled?	Yes
		Minor Editing Privileges?	Yes
Who Will Republish the Content?	Academic institution	Incidental Promotional Use?	No
Duration of Use	Life of current edition	Currency	USD
Lifetime Unit Quantity	Up to 499		
Rights Requested	Main product		

License Number: 5663140371208

ELSEVIER LICENSE
TERMS AND CONDITIONS

Nov 06, 2023

This Agreement between Victoria Bishop ("You") and Elsevier ("Elsevier") consists of your license details and the terms and conditions provided by Elsevier and Copyright Clearance Center.

License Number	5663140371208
License date	Nov 06, 2023
Licensed Content Publisher	Elsevier
Licensed Content Publication	Nano Energy
Licensed Content Title	A flexible solar cell/supercapacitor integrated energy device
Licensed Content Author	Pei Dong,Marco-Tulio F. Rodrigues,Jing Zhang,Raquel S. Borges,Kaushik Kalaga,Arava L.M. Reddy,Glaura G. Silva,Pulickel M. Ajayan,Jun Lou
Licensed Content Date	Dec 1, 2017
Licensed Content Volume	42
Licensed Content Issue	n/a
Licensed Content Pages	6
Start Page	181
End Page	186

APPENDIX (continued.)

License Number: 1413772-1

Order Date	06-Nov-2023	Type of Use	Republish in a thesis/dissertation
Order License ID	1413772-1		
ISSN	2398-4902	Publisher	Royal Society of Chemistry
		Portion	Image/photo/illustration

LICENSED CONTENT

Publication Title	Sustainable Energy & Fuels	Rightsholder	Royal Society of Chemistry
Article Title	High energy and high voltage integrated photo-electrochemical double layer capacitor	Publication Type	e-Journal
		Start Page	968
		End Page	977
		Issue	5
Author/Editor	Royal Society of Chemistry (Great Britain)	Volume	2
Date	01/01/2016		
Language	English		
Country	United Kingdom of Great Britain and Northern Ireland		

REQUEST DETAILS

Portion Type	Image/photo/illustration	Distribution	United States
Number of Images / Photos / Illustrations	1	Translation	Original language of publication
Format (select all that apply)	Electronic	Copies for the Disabled?	Yes
		Minor Editing Privileges?	Yes
Who Will Republish the Content?	Academic institution	Incidental Promotional Use?	No
Duration of Use	Life of current edition	Currency	USD
Lifetime Unit Quantity	Up to 499		
Rights Requested	Main product		

License Number: 5663140229966

ELSEVIER LICENSE
TERMS AND CONDITIONS

Nov 06, 2023

This Agreement between Victoria Bishop ("You") and Elsevier ("Elsevier") consists of your license details and the terms and conditions provided by Elsevier and Copyright Clearance Center.

License Number	5663140229966
License date	Nov 06, 2023
Licensed Content Publisher	Elsevier
Licensed Content Publication	Energy
Licensed Content Title	Innovative multipolymer electrolyte membrane designed by oxygen inhibited UV-crosslinking enables solid-state in plane integration of energy conversion and storage devices
Licensed Content Author	Alberto Scalia,Federico Bella,Andrea Lamberti,Claudio Gerbaldi,Elena Tresso
Licensed Content Date	Jan 1, 2019
Licensed Content Volume	166
Licensed Content Issue	n/a
Licensed Content Pages	7
Start Page	789

APPENDIX (continued.)

License Number: 5663140612935

ELSEVIER LICENSE
TERMS AND CONDITIONS

Nov 06, 2023

This Agreement between Victoria Bishop ("You") and Elsevier ("Elsevier") consists of your license details and the terms and conditions provided by Elsevier and Copyright Clearance Center.

License Number	5663140612935
License date	Nov 06, 2023
Licensed Content Publisher	Elsevier
Licensed Content Publication	Applied Materials Today
Licensed Content Title	Redox active and electrically conducting cobalt telluride Nanorods/Poly(1-aminoanthraquinone) composite and photoactive Rose Bengal dye based photo-supercapacitor
Licensed Content Author	Aparajita Das,Sathish Deshagani,Partha Ghosal,Melepurath Deepa
Licensed Content Date	Jun 1, 2020
Licensed Content Volume	19
Licensed Content Issue	n/a
Licensed Content Pages	1
Start Page	100592

License Number: 5663140721744

ELSEVIER LICENSE
TERMS AND CONDITIONS

Nov 06, 2023

This Agreement between Victoria Bishop ("You") and Elsevier ("Elsevier") consists of your license details and the terms and conditions provided by Elsevier and Copyright Clearance Center.

License Number	5663140721744
License date	Nov 06, 2023
Licensed Content Publisher	Elsevier
Licensed Content Publication	Science Bulletin
Licensed Content Title	Selected functionalization of continuous graphene fibers for integrated energy conversion and storage
Licensed Content Author	Yao Yao,Tian Lv,Ning Li,Zilin Chen,Chi Zhang,Tao Chen
Licensed Content Date	Mar 30, 2020
Licensed Content Volume	65
Licensed Content Issue	6
Licensed Content Pages	10
Start Page	486

APPENDIX (continued.)

License Number: 5663140813788

JOHN WILEY AND SONS LICENSE
TERMS AND CONDITIONS

Nov 06, 2023

This Agreement between Victoria Bishop ("You") and John Wiley and Sons ("John Wiley and Sons") consists of your license details and the terms and conditions provided by John Wiley and Sons and Copyright Clearance Center.

License Number	5663140813788
License date	Nov 06, 2023
Licensed Content Publisher	John Wiley and Sons
Licensed Content Publication	Angewandte Chemie
Licensed Content Title	An Integrated "Energy Wire" for both Photoelectric Conversion and Energy Storage
Licensed Content Author	Huisheng Peng, Xuemei Sun, Huijuan Lin, et al
Licensed Content Date	Oct 29, 2012
Licensed Content Volume	124
Licensed Content Issue	48
Licensed Content Pages	4
Type of use	Dissertation/Thesis
Requestor type	University/Academic

License Number: 1413772-3

Order Date	06-Nov-2023	Type of Use	Republish in a thesis/dissertation
Order License ID	1413772-3		
ISSN	1754-5706	Publisher	RSC Publishing
		Portion	Image/photo/illustration

LICENSED CONTENT

Publication Title	Energy & environmental science	Rightsholder	Royal Society of Chemistry
		Publication Type	e-Journal
Article Title	Integrated power fiber for energy conversion and storage	Start Page	805
		Issue	3
Author/Editor	Royal Society of Chemistry (Great Britain)	Volume	6
		URL	http://www.rsc.org/Publishing/Journals/EE/Index.asp
Date	01/01/2008		
Language	English		
Country	United Kingdom of Great Britain and Northern Ireland		

REQUEST DETAILS

Portion Type	Image/photo/illustration	Distribution	United States
Number of Images / Photos / Illustrations	1	Translation	Original language of publication
Format (select all that apply)	Electronic	Copies for the Disabled?	Yes
		Minor Editing Privileges?	Yes
Who Will Republish the Content?	Academic institution	Incidental Promotional Use?	No
Duration of Use	Life of current edition	Currency	USD
Lifetime Unit Quantity	Up to 499		
Rights Requested	Main product		